

1        **Coupled Stratospheric Ozone and Atlantic Meridional Overturning**  
2        **Circulation Feedbacks on the Northern Hemisphere Midlatitude Jet**  
3        **Response to 4xCO<sub>2</sub>**

4 Clara Orbe<sup>a,b</sup>, David Rind<sup>a</sup>, Darryn Waugh<sup>c</sup>, Jeffrey Jonas<sup>a,d</sup>, Xiyue Zhang<sup>c</sup>, Gabriel Chiodo<sup>e</sup>,  
5 Larissa Nazarenko<sup>a,d</sup>, and Gavin A. Schmidt<sup>a</sup>

6                    <sup>a</sup> *NASA Goddard Institute for Space Studies, New York, NY*

7                    <sup>b</sup> *Department of Applied Physics and Applied Mathematics, Columbia University, New York, NY*

8                    <sup>c</sup> *Department of Earth and Planetary Sciences, Johns Hopkins University, Baltimore, MD*

9                    <sup>d</sup> *Center for Climate Systems Research, Earth Institute, Columbia University, New York, NY*

10                    <sup>e</sup> *Institute for Atmospheric and Climate Science, ETH Zurich, Switzerland*

12 ABSTRACT: Stratospheric ozone, and its response to anthropogenic forcings, provide an im-  
13 portant pathway for the coupling between atmospheric composition and climate. In addition to  
14 stratospheric ozone's radiative impacts, recent studies have shown that changes in the ozone layer  
15 due to  $4xCO_2$  have a considerable impact on the Northern Hemisphere (NH) tropospheric circula-  
16 tion, inducing an equatorward shift of the North Atlantic jet during boreal winter. Here we show  
17 that this equatorward jet shift can induce a more rapid weakening of the Atlantic Meridional Over-  
18 turning Circulation (AMOC), resulting in a poleward shift of the midlatitude eddy-driven jet on  
19 longer timescales. As such, coupled feedbacks from both stratospheric ozone and the AMOC result  
20 in a two-timescale response of the NH midlatitude jet to abrupt  $4xCO_2$  forcing: a "fast" response  
21 (5-20 years) during which it shifts equatorward and a "total" response ( $\sim 100$ -150 years) during  
22 which the jet shifts poleward. The latter is driven by a weakening of the AMOC that develops  
23 in response to weaker surface zonal winds, that result in reduced heat fluxes out of the subpolar  
24 gyre and reduced North Atlantic Deep Water formation. Our results suggest that stratospheric  
25 ozone changes in the lower stratosphere can have a surprisingly powerful effect on the AMOC,  
26 independent of other aspects of climate change.

## 27 **1. Introduction**

28 There is large uncertainty in the atmospheric circulation response to increasing greenhouse gases  
29 (see Shepherd (2014) and references therein). Although models generally predict a poleward shift  
30 of the midlatitude eddy-driven jet, the magnitude of this shift is highly uncertain (e.g., Vallis et al.  
31 (2015); Grise and Polvani (2014)) as are its underlying drivers (Shaw (2019)). This is especially  
32 true in the Northern Hemisphere (NH), where there are opposing thermodynamic influences, i.e.  
33 opposite meridional temperature gradient responses at the surface versus the upper troposphere  
34 (Shaw et al. (2016)). Thus, while enhanced warming in the lower polar troposphere relative  
35 to the lower tropical troposphere (i.e., Arctic amplification) contributes to reduced meridional  
36 temperature gradients, increases in upper tropospheric tropical warming contribute to enhanced  
37 temperature gradients aloft (Butler et al. (2010); Yuval and Kaspi (2020)) and it is not clear how  
38 these competing processes affect the zonal mean midlatitude jet.

39 Many processes have been shown to influence the response of meridional temperature gradients  
40 to increased CO<sub>2</sub>, including polar amplification (see Smith et al. (2019) and references therein)  
41 and cloud feedbacks (e.g., Ceppi and Hartmann (2015); Voigt and Shaw (2015)). By comparison,  
42 composition feedbacks associated with the ozone response to CO<sub>2</sub> have been less well examined  
43 although stratospheric ozone changes have been identified as an important pathway coupling  
44 composition to climate (Isaksen et al. (2009)). In particular, the stratospheric ozone response to  
45 4xCO<sub>2</sub> consists of robust decreases in the tropical lower stratosphere (LS), increases in the tropical  
46 upper stratosphere and increases over high latitudes (Chiodo et al. (2018)). While the exact details  
47 of these changes are model dependent, especially over high latitudes, the general pattern is very  
48 consistent among models (e.g., Nowack et al. (2015); Chiodo et al. (2018) and Chiodo and Polvani  
49 (2019) (hereafter CP2019)).

50 This pattern of reduced (increased) ozone over the tropical (high latitude) LS in response to  
51 4xCO<sub>2</sub> has immediate implications for temperature gradients in the stratosphere by cooling the  
52 tropics and warming high latitudes (Nowack et al. (2015); Chiodo et al. (2018); Li and Newman  
53 (2022)). As CP2019 and Li and Newman (2022) showed, these changes in temperature gradients  
54 drive an anomalous equatorward shift of the midlatitude jet in the Southern Hemisphere (SH).  
55 In addition, both studies also showed shifts in the Northern Hemisphere (NH), where anomalies

56 extend down into the lower troposphere and are concentrated over the Atlantic, resembling the  
57 negative phase of the North Atlantic Oscillation (NAO).

58 A more recent study by Zhang et al. (2023), that considered two models that differed only in  
59 their representation of interactive chemistry, also showed that changes in composition can impact  
60 the sign of the NH midlatitude jet response to increased CO<sub>2</sub>. However, in contrast to CP2019,  
61 the long-term impact of this composition feedback was a *poleward*, not equatorward, shift of the  
62 NH jet. Though not investigated in detail, this poleward shift of the jet was linked to changes in  
63 the ocean circulation, which were not examined in CP2019. More precisely, Zhang et al. (2023)  
64 noted that the Atlantic Meridional Overturning Circulation (AMOC) exhibited a stronger decline  
65 in interactive simulations in which trace gases and aerosols were allowed to respond to increased  
66 CO<sub>2</sub>, relative to non-interactive simulations. Indeed, recent studies have highlighted the large  
67 influence that changes in the AMOC exert on the response of the NH midlatitude jet to increased  
68 CO<sub>2</sub> (Gervais et al. (2019)), with models featuring a larger AMOC decline also tending to produce  
69 a stronger poleward jet shift (Bellomo et al. (2021); Liu et al. (2020); Orbe et al. (2023)).

70 The results from Zhang et al. (2023) suggest that composition feedbacks on the NH midlatitude  
71 jet may depend on the response of the ocean circulation. However, that study did not examine the  
72 mechanism underlying the stronger AMOC response in the interactive chemistry simulations nor  
73 did it isolate the role of ozone from influences due to other trace gases and aerosols. To this end,  
74 here we hypothesize that the ozone-induced negative NAO wind anomalies reported in CP2019  
75 provide a potential pathway through which stratospheric ozone changes can influence the AMOC  
76 and the long-term response of the NH midlatitude jet. Our hypothesis is partly predicated on results  
77 from previous studies showing that variations in the jet – namely those resembling the NAO – can  
78 influence variability of the AMOC through changes in wind stress (Marshall et al. (2001); Zhai and  
79 Marshall (2014)). Modified air-sea fluxes of heat, water and momentum associated with variations  
80 in the NAO alter vertical and horizontal density gradients in the subpolar gyre, inducing changes  
81 in deep water formation and the AMOC (e.g., Visbeck et al. (1998); Delworth and Dixon (2000)).  
82 This pathway via the NAO has been used to demonstrate how sudden stratospheric warmings  
83 influence the variability of heat flux anomalies into the ocean and ocean mixed layer depths in  
84 the North Atlantic (O’Callaghan and Mitchell (2014)) as well as the strength of the AMOC itself  
85 (Reichler et al. (2012)).

86 Here we present results from non-interactive and fully interactive chemistry global warming  
87 experiments produced with the new high-top coupled atmosphere ocean version of the NASA  
88 Goddard Institute for Space Studies (GISS) climate model that were submitted to the Coupled  
89 Model Intercomparison Project Phase 6 (CMIP6) (Eyring et al. (2016)). We focus on simulations  
90 in which CO<sub>2</sub> is abruptly doubled and quadrupled in order to facilitate comparison with the results  
91 presented in CP2019 and Zhang et al. (2023).

92 We begin by verifying that reduced ozone in the tropical lower stratosphere, which is captured  
93 only in the interactive simulations, leads to an equatorward shift of the midlatitude jet on relatively  
94 fast timescales. Then we show that the AMOC response in the interactive simulations is largely  
95 associated with these ozone-driven changes in the jet, not aerosols, using new experiments in  
96 which the stratospheric ozone response to 4xCO<sub>2</sub> is isolated from changes in other trace gases and  
97 aerosols. In particular, we show that our model captures the ozone-induced negative NAO-like  
98 pattern first reported in CP2019; in addition, we also find that ozone-driven changes in surface  
99 friction speed further weaken the AMOC, resulting in a long-term poleward shift of the NH jet.  
100 As a result, we show that both stratospheric ozone changes and the AMOC influence the NH jet on  
101 distinct “fast” and “total” timescales (and in the opposite sense), comprising a coupled atmosphere-  
102 ocean feedback on the NH midlatitude jet response to increased CO<sub>2</sub>. While the former “fast”  
103 feedback was documented in CP2019, the latter has, to the best of our knowledge, not been reported  
104 in previous studies.

105 It is important to note that previous studies have long shown that interactive atmospheric compo-  
106 sition can strongly influence the AMOC, placing an almost exclusive focus on the role of aerosols  
107 (Booth et al. (2012); Cowan and Cai (2013); Swingedouw et al. (2015)). More recently, Rind  
108 et al. (2018) also identified a larger sensitivity of the AMOC response to global warming using an  
109 interactive configuration of the CMIP5 version of the GISS climate model (GISS-E2-R), compared  
110 to a non-interactive version. In that study, multicentennial cessations of the AMOC were found to  
111 occur in simulations in which natural aerosols (primarily sea salt) were allowed to locally cool sea  
112 surface temperatures through their influence on cloud optical thickness; these cooler SSTs were  
113 then linked to reduced evaporation relative to precipitation, resulting in positive surface freshwater  
114 forcing and reduced NADW production. As in Rind et al. (2018) we also show that composition  
115 feedbacks play an important role on the response of the AMOC to CO<sub>2</sub> through their influence

116 on surface fluxes and surface temperatures. However, the mechanism proposed here only invokes  
117 changes in stratospheric ozone, not aerosols. We begin by discussing methods in Section 2 and  
118 then present key results and conclusions in Sections 3 and 4, respectively.

## 119 **2. Methods**

### 120 *a. Model and Configurations*

121 Here we use the NASA Goddard Institute for Space Studies (GISS) “Middle Atmosphere (MA)”  
122 Model E2.2 (Rind et al. (2020); Orbe et al. (2020)). E2.2 consists of 102 vertical levels spanning  
123 the surface up to 0.002 hPa and is run at a horizontal resolution of 2 degrees by 2.5 degrees.  
124 Orographic and non-orographic gravity wave drag is parameterized following Lindzen (1987)  
125 and Rind et al. (1988), producing in E2.2 a quasibiennial oscillation (QBO) that compares well  
126 with observations as well as improved stratospheric polar vortex variability (Ayarzagüena et al.  
127 (2020); Rind et al. (2020)). Of most relevance to this study, Orbe et al. (2020) showed that E2.2  
128 produces a significantly improved representation of the Brewer-Dobson and stratospheric transport  
129 circulations, compared to the lower vertical resolution CMIP6 version of ModelE (E2.1, Kelley  
130 et al. (2020)), resulting in reduced biases in ozone, methane, water vapor and nitrous oxide (see  
131 their Figure 1). Among the different model versions discussed in Rind et al. (2020) and Orbe  
132 et al. (2020) here we focus on the “Altered-Physics” (-AP) Version (E2.2-AP) because this is the  
133 configuration that was submitted to CMIP6 and presented in recent studies (Ayarzagüena et al.  
134 (2020); DallaSanta et al. (2021a,b)).

135 We begin by showing the results reported in Zhang et al. (2023) using both “Non-INTeractive”  
136 (NINT) (Table 1, rows 1-3) and fully interactive “One-Moment Aerosols” (OMA) (Bauer et al.  
137 (2020); Table 1, rows 4-6) configurations. In the NINT configuration all trace gases and aerosols  
138 are set to preindustrial values. Hence, in the 2- and 4xCO<sub>2</sub> NINT runs neither ozone nor other trace  
139 gases (besides water vapor) change in response to increased CO<sub>2</sub>. By comparison, the OMA 2- and  
140 4xCO<sub>2</sub> runs capture the full nonlinear ozone response to CO<sub>2</sub>, as well as composition feedbacks  
141 associated with other trace gases and aerosols.

142 In order to isolate the role of ozone feedbacks on the circulation, we then perform experiments  
143 using a linearized ozone (LINOZ) configuration (Table 1, rows 7-9). In LINOZ the ozone field is  
144 calculated interactively by Taylor expanding the equation of state around present-day (2000–2010)

154 TABLE 1. The Model E2.2 experiments presented in this study, including preindustrial control, abrupt 2xCO<sub>2</sub>  
 155 and abrupt 4xCO<sub>2</sub> simulations using NINT (rows 1-3), OMA (rows 4-6) and LINOZ (rows 7-9) configurations.  
 156 Four NINT abrupt 4xCO<sub>2</sub> ensemble members are included (row 3) in order to compare with a four member  
 157 4xCO<sub>2</sub> ensemble produced using the LINOZ configuration (row 8). The 4xCO<sub>2</sub> ensemble mean LINOZ ozone  
 158 response is also used to force four prescribed SST and SIC preindustrial experiments (row 10) in which all  
 159 forcings other than ozone are set to preindustrial values. All coupled atmosphere-ocean simulations are run using  
 160 the GISS Ocean v1 (GO1) (i.e., “-G” in CMIP6 notation).

Configuration	Ozone	CO <sub>2</sub>	Ensemble Size	SSTs and SICs
NINT	Preindustrial	Preindustrial	1	coupled (-G ocean)
NINT	Preindustrial	2xCO <sub>2</sub>	1	coupled (-G ocean)
NINT	Preindustrial	4xCO <sub>2</sub>	4	coupled (-G ocean)
OMA	Preindustrial	Preindustrial	1	coupled (-G ocean)
OMA	2xCO <sub>2</sub>	2xCO <sub>2</sub>	1	coupled (-G ocean)
OMA	4xCO <sub>2</sub>	4xCO <sub>2</sub>	1	coupled (-G ocean)
LINOZ	Preindustrial	Preindustrial	1	coupled (-G ocean)
LINOZ	2xCO <sub>2</sub>	2xCO <sub>2</sub>	1	coupled (-G ocean)
LINOZ	4xCO <sub>2</sub>	4xCO <sub>2</sub>	4	coupled (-G ocean)
NINT	LINOZ 4xCO <sub>2</sub>	Preindustrial	4	Prescribed Preindustrial

145 values such that the ozone tendency is, to first-order, parameterized as a function of the local ozone  
 146 mixing ratio, temperature, and overhead column ozone (McLinden et al. (2000)). Tropospheric  
 147 ozone is calculated using monthly mean ozone production and loss rates archived from GEOS-  
 148 CHEM (Rind et al. (2014)). In contrast to NINT, therefore, the LINOZ ensemble captures the  
 149 influence of the ozone response to CO<sub>2</sub> on the large-scale circulation. Unlike OMA, however, it is  
 150 much more computationally efficient to run and isolates the ozone feedback from feedbacks related  
 151 to other trace gases and aerosols. DallaSanta et al. (2021a) previously showed that the LINOZ  
 152 ozone parameterization reproduces well the vertical structure and seasonal cycle of stratospheric  
 153 ozone obtained from the fully interactive OMA configuration (see their Figure 1).

### 161 *b. Experiments*

162 For the different model configurations (NINT, OMA, LINOZ) we perform 150-year-long abrupt  
 163 2- and 4xCO<sub>2</sub> experiments, in which CO<sub>2</sub> values are abruptly doubled and quadrupled relative to  
 164 preindustrial concentrations. For each model configuration, these experiments are branched from

165 a corresponding preindustrial control simulation. For NINT and LINOZ four-member  $4\times\text{CO}_2$   
166 ensembles are run in order to assess the robustness of any ozone feedbacks. These experiments are  
167 all conducted using the atmosphere-ocean version of E2.2-AP that is coupled to the GISS Ocean  
168 v1 (GO1) (i.e., “-G” in CMIP6 notation, hereafter simply E2.2-G). For coupled atmosphere-ocean  
169 configurations in which (four-member) ensembles are run, different ensemble members are chosen  
170 from different initial ocean states spaced 20 years apart in the corresponding preindustrial control  
171 simulation.

172 In addition to the coupled atmosphere-ocean experiments, we also present results from a four-  
173 member ensemble of 60-year-long atmosphere-only experiments in which sea surface temperatures  
174 (SSTs) and sea ice concentrations (SICs) are fixed to preindustrial values, but the monthly mean  
175 time-evolving ensemble mean ozone response from the coupled LINOZ  $4\times\text{CO}_2$  experiments is  
176 prescribed (Table 1, row 10). This allows us to quantify the impact of the ozone feedback  
177 represented in LINOZ on the large-scale circulation, absent any contributions from changes in  
178 background  $\text{CO}_2$ , sea ice concentrations or sea surface temperatures.

### 179 *c. Analysis*

#### 180 1) TIMESCALES

181 When examining the midlatitude jet response to increased  $\text{CO}_2$  we account for the fact that  
182 extratropical circulation changes consist of distinct “fast” and “slow” responses (Ceppi et al. (2018),  
183 hereafter CZS2018). More precisely, CZS2018 show that most of the shift of the midlatitude jets  
184 occurs within 5-10 years of a steplike (abrupt)  $\text{CO}_2$  forcing, with little shifts occurring during a  
185 slower response over which SSTs change over subsequent decades. In contrast to the Southern  
186 Hemisphere, zonal asymmetries play an important role in the Northern Hemisphere, where the  
187 influence of local patterns in sea surface temperature change can result in oppositely signed jet  
188 shifts on “slow” timescales. Given this potential for compensating jet shifts on distinct timescales,  
189 we therefore decompose the  $\text{CO}_2$  circulation response into “fast” and “total” timescale responses.

190 More precisely, to account for the large internal variability in our runs, perhaps related to a  
191 somewhat larger ENSO amplitude in our model compared to observations (Rind et al. (2020)),  
192 we modify the original approach used in CZS2018 to define our “fast” response as the difference  
193 between the ensemble mean  $4\times\text{CO}_2$  response, averaged over years 5-20 (as opposed to years 5-10),

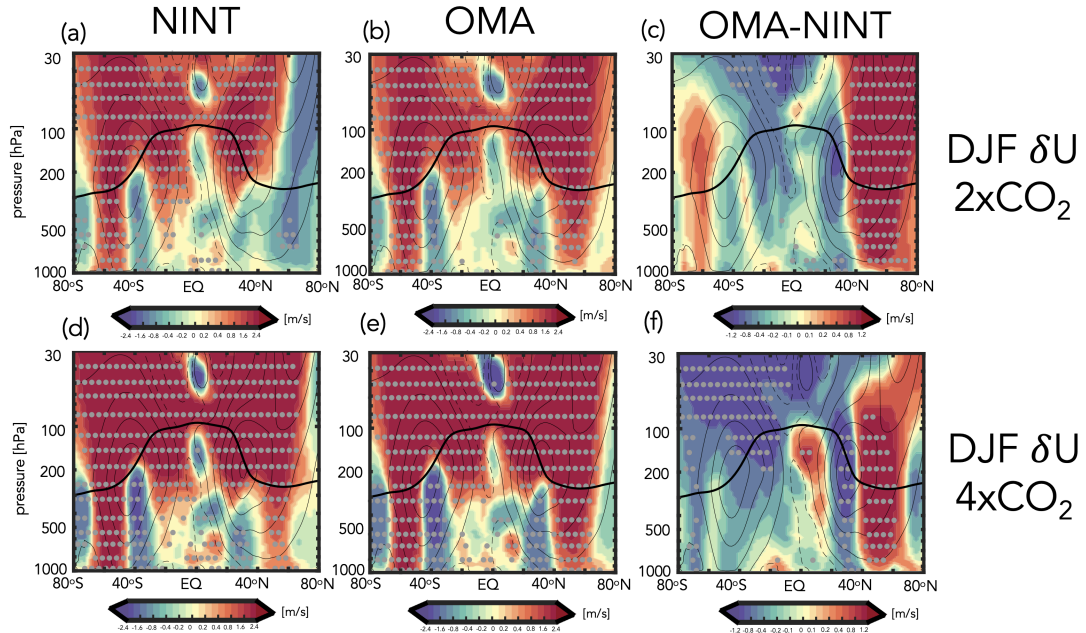


194 and the corresponding preindustrial control simulation. In addition, instead of focusing on the  
195 “slow” response, defined in CZS2018 as the difference between averages over years 121-140 and  
196 years 5-10, here we examine the “total” response, defined as the difference between the ensemble  
197 mean  $4\times\text{CO}_2$  response, averaged over years 100-150, and the preindustrial control simulation. This  
198 approach is more consistent with what was used in Zhang et al. (2023) and CP2019, with which  
199 we directly compare our results throughout. Note that in response to an abrupt quadrupling of  
200  $\text{CO}_2$  the NINT model configuration produces global mean surface temperature “fast” and “total”  
201 responses of  $\sim 2.9^\circ\text{C}$  and  $\sim 3.9^\circ\text{C}$ , respectively. Statistical significance is assessed using a two-  
202 sample Student’s t-test comparing all abrupt  $\text{CO}_2$  changes to the interannual variability in the  
203 corresponding preindustrial control simulation for each configuration (Table 1, rows 1,4,7).

## 204 2) ANALYSIS FIELDS

205 In addition to the atmospheric variables examined in CP2019 (i.e., zonal mean wind, zonal mean  
206 temperature, surface temperature, 850 hPa zonal wind) we examine ocean variables relevant to  
207 understanding the evolution of the AMOC and its coupling to the atmosphere. In particular, in  
208 addition to examining the surface mixed layer depths we also examine sea surface temperatures,  
209 surface friction speed, horizontal ocean heat and salinity transports, as well as the net heat fluxes  
210 which, together with the net freshwater fluxes ( $F$ ; inferred from precipitation minus evaporation  
211 ( $P-E$ )), provide information about the surface buoyancy forcing (Large and Yeager (2009)). In our  
212 simulations, the preindustrial climatological buoyancy forcing over the North Atlantic is dominated  
213 by the sum of the net heat fluxes ( $Q = Q_H + Q_E + Q_S + Q_L$ ), which are defined to be positive into the  
214 ocean (Appendix Figure A1, left). These are further partitioned into their respective latent heat  
215 ( $Q_E$ ) and sensible heat ( $Q_H$ ) contributions as we find that the net solar ( $Q_S$ ) and longwave ( $Q_L$ ) flux  
216 radiative contributions are negligible over the North Atlantic region (Appendix Figure A1, right).

217 Given our interest in the Northern Hemisphere we focus primarily on December-January-  
218 February (DJF). The ocean heat transport changes in our simulations are also most pronounced  
219 during DJF, consistent with the analyses presented in Romanou et al. (2023) and Orbe et al. (2023).



229 FIG. 1. Colors show the December-January-February (DJF) response of the zonal mean zonal winds,  $U$ , to  
 230 an abrupt doubling (top) and quadrupling (bottom) of  $\text{CO}_2$ , averaged over years 100-150. Results are shown  
 231 for NINT (a,d) and fully interactive OMA configurations (b,e), where one ensemble member has been used for  
 232 each forcing scenario. The OMA - NINT differences are also shown (c,f). Black contours denote climatological  
 233 mean preindustrial control DJF  $U$  values (contour interval: 8 m/s). Stippled regions are statistically significant  
 234 and the black thick line shows the climatological mean tropopause in the preindustrial control NINT simulation.  
 235 Note that all colorbar bounds are consistent with those used in Chiodo and Polvani (2019) in order to facilitate  
 236 comparisons with that study.

### 220 3. Results

#### 221 a. Abrupt $2x\text{CO}_2$ and $4x\text{CO}_2$ Zonal Mean Wind Response: OMA versus NINT

222 Before focusing on ozone feedbacks, we first review the OMA versus NINT differences in NH  
 223 jet behavior that were presented in Zhang et al. (2023) (Figure 1). In the stratosphere the zonally  
 224 averaged DJF wind response to 2- and  $4x\text{CO}_2$  features an acceleration at nearly all latitudes,  
 225 consistent with amplified warming in the tropical upper troposphere (Shaw (2019)) and increased  
 226 cooling of the stratosphere with height (Garcia and Randel (2008)). Similar wind responses emerge  
 227 in both the NINT and OMA configurations, except over northern high latitudes at  $2x\text{CO}_2$ , where  
 228 the strengthened zonal winds in NINT are not statistically significant.

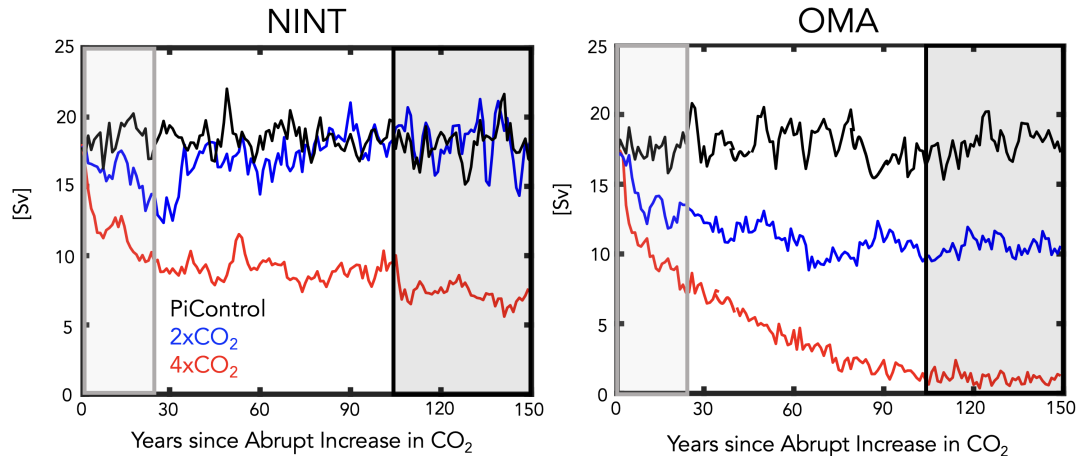
237 In the troposphere, however, there are noticeable differences between the OMA and NINT  
238 simulations. In particular, the NH midlatitude jet features a much stronger poleward shift in OMA,  
239 compared to NINT (Figures 3 and 6 in Zhang et al. (2023)). As discussed in that study, the stronger  
240 response in OMA results in enhanced eddy mixing along isentropes on the poleward flank of the  
241 NH jet, resulting in increased transport of tracers from the northern midlatitude surface to the  
242 Arctic (not shown). This difference between OMA and NINT occurs at both 2- and at 4xCO<sub>2</sub>,  
243 resulting in a nonlinearity in the jet (and tracer transport) response in NINT that is not present in  
244 the OMA simulations. In the SH, by comparison, the differences between OMA and NINT are  
245 much smaller and not statistically significant.

246 Zhang et al. (2023) hypothesized that the nonlinearity in NH jet behavior evident in the “total”  
247 response in the NINT model configuration was related to a nonlinear AMOC response to CO<sub>2</sub>  
248 forcing (Figure 2). That is, despite an initial weakening, the AMOC eventually recovers to  
249 preindustrial values in the NINT 2xCO<sub>2</sub> simulation, in contrast to the total response to 4xCO<sub>2</sub>  
250 in which the AMOC is about 10 SV weaker than the preindustrial control (Fig. 2, left, black  
251 box). This results in a so-called “AMOC nonlinearity” to CO<sub>2</sub> forcing of ~-5SV in the NINT  
252 configuration. By comparison, in the OMA configuration, the AMOC weakens by ~7 and ~17 SV  
253 in the 2- and 4xCO<sub>2</sub> simulations, respectively, representing only a very weak nonlinearity in the  
254 long-term response of the AMOC (of ~1.5 SV) (Fig. 2, right, black box).

259 As it is difficult to meaningfully interpret the zonal mean wind response in the NH, where there  
260 are large zonal variations in the midlatitude jet (Simpson et al. (2014)), we next compare the 850  
261 hPa zonal wind changes between the NINT and OMA 4xCO<sub>2</sub> simulations, further distinguishing  
262 between “fast” and “total” responses (Figure 3). We begin with the NINT equilibrated or “total”  
263 response (i.e. years 100-150), which consists of a poleward jet shift over the Pacific basin and an  
264 acceleration and eastward extension of the jet over the Atlantic and Eurasia (Fig. 3b). This pattern  
265 is amplified in the OMA run (Fig. 3d), in which both the strengthening and eastward extension of  
266 the jet over the Atlantic and its poleward shift over the Pacific are more pronounced. This amplified  
267 response in OMA over both the Pacific and Eurasia is also evident at 300 hPa (Appendix Figure  
268 A2b).

269 This wind response in OMA, relative to NINT, is consistent with the jet differences identified in  
270 Orbe et al. (2023) between two non-interactive simulations of the GISS low-top climate model in

## Annual Mean AMOC Response at 48°N



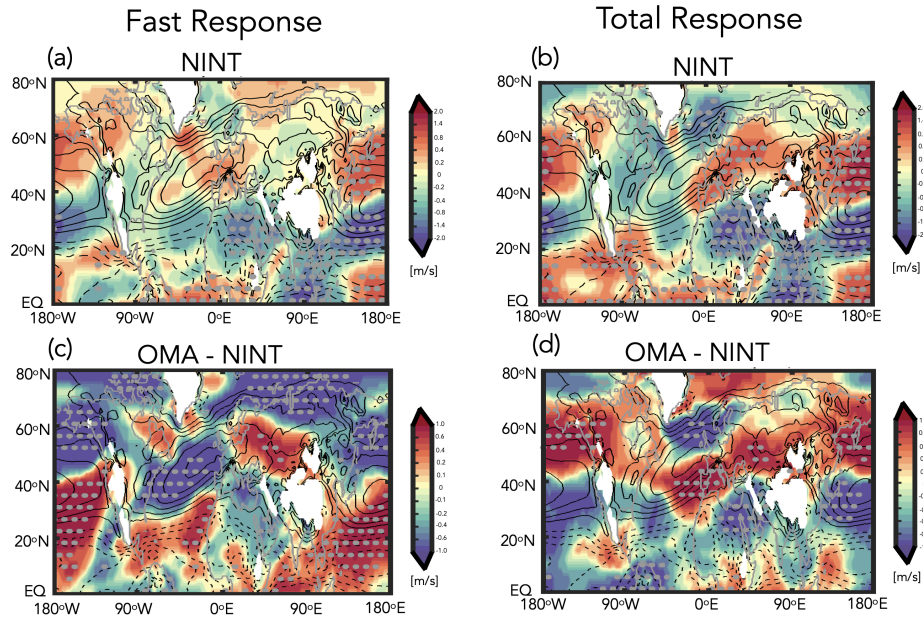
255 FIG. 2. Evolution of the annual mean maximum overturning stream function in the Atlantic ocean, evaluated  
 256 at 48°N, for the preindustrial control (black), abrupt 2xCO<sub>2</sub> (blue) and abrupt 4xCO<sub>2</sub> (red) simulations. Results  
 257 for the NINT (left) and OMA (right) configurations are shown. Light grey and black shaded boxes denote the  
 258 “fast” and “total” timescale response averaging periods.

271 which only the AMOC strength differed. This suggests that the jet differences between OMA and  
 272 NINT on these longer timescales are primarily driven by differences in the AMOC response, as  
 273 hypothesized in Zhang et al. (2023).

280 Figure 2 (grey boxes) highlights how the AMOC differences between OMA and NINT noted  
 281 in Zhang et al. (2023) arise very early in the simulations (within the first 20 years). Over these  
 282 years – which comprise the “fast” response – the impact of interactive chemistry on the zonal  
 283 wind changes at 850 hPa is very different (Fig. 3a,c). In particular, over the Atlantic, interactive  
 284 composition results in a strong weakening over the midlatitude jet core and an acceleration on the  
 285 equatorward flank of the jet (Fig. 3c). This wind change is also evident at 300 hPa (not examined  
 286 in CP2019), where the winds accelerate on the equatorward and poleward flanks of the midlatitude  
 287 and subtropical jets, respectively (Fig. A2a). Over the Pacific, where the midlatitude jet is more  
 288 vertically coherent, interactive chemistry results in an anomalous equatorward jet shift relative to  
 289 the NINT simulation at both 850 hPa (Fig. 3a) and 300 hPa (Fig. A2a).

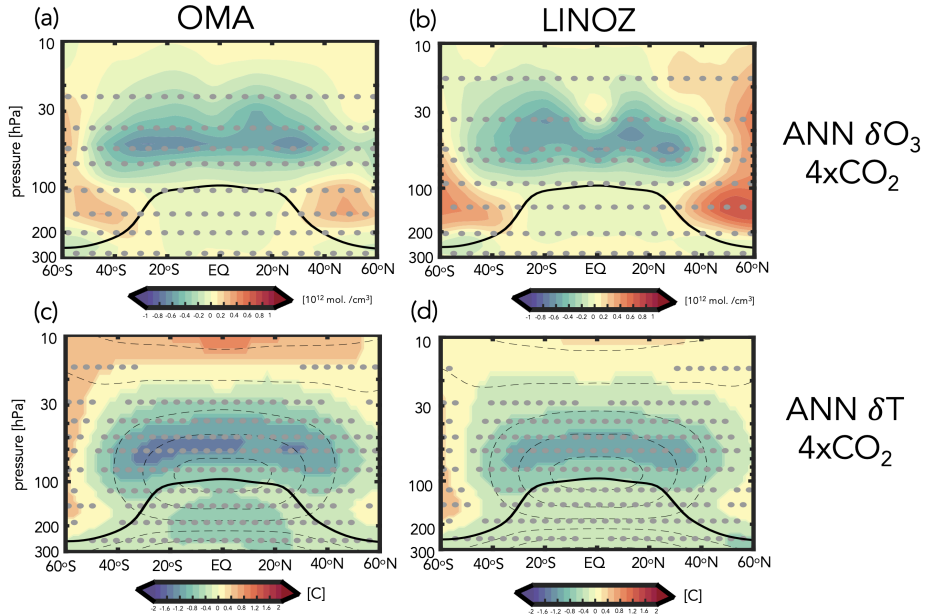
290 This fast composition feedback that occurs over years 5-20 is consistent with the results from  
 291 CP2019, who showed that the ozone response to 4xCO<sub>2</sub> induces a weakening of the North Atlantic

## DJF 4xCO<sub>2</sub> $\delta U$ at 850 hPa



274 FIG. 3. Colors show the 4xCO<sub>2</sub> (four member) ensemble mean change in the DJF 850 hPa zonal winds  
 275 for the NINT configuration, decomposed into “fast” (i.e. years 5-20) (a) and “total” (i.e. years 100-150) (b)  
 276 responses. The OMA - NINT fast and total differences are shown in (c) and (d), respectively. Note that one  
 277 ensemble member is used in displaying the OMA - NINT differences (same as used in Figure 1). Black contours  
 278 denote climatological mean preindustrial control DJF values (U contour interval: 2 m/s) and stippled regions are  
 279 statistically significant.

292 jet and a strengthening on its equatorward flank (see their Figure 6). This response is reminiscent  
 293 of the negative phase of the NAO which previous studies have shown can result in a weaker  
 294 AMOC (Delworth and Zeng (2016)). In CP2019, however, this response is realized through  
 295 changes in stratospheric ozone alone, whereas in OMA all trace gases and aerosols are responding.  
 296 Furthermore, the significance of this rapid response with only one ensemble member is uncertain,  
 297 particularly during the first 5-20 years when the signal is confounded by large internal variability.  
 298 To this end, next we present results from the larger (4-member) LINOZ ensemble to examine  
 299 whether the fast response in the NH jet is related to stratospheric ozone changes.



311 FIG. 4. Colors show the annual averaged change in ozone number density (top) and temperature (bottom)  
 312 in response to  $4xCO_2$ . Results for OMA (left) and LINOZ (right) are shown, averaged over years 5-20. One  
 313 simulation is shown for OMA and the four-member ensemble mean response is shown for LINOZ. Black  
 314 contours in the bottom panels show climatological mean preindustrial control temperatures (contour interval: 10  
 315 C). Stippled regions are statistically significant and the black thick line shows the climatological mean tropopause  
 316 in the preindustrial control NINT simulation.

300 *b. Abrupt  $4xCO_2$  Stratospheric Ozone and Temperature Responses: OMA versus LINOZ*

301 Before examining the circulation response in the LINOZ ensemble, we first compare the annually  
 302 averaged ensemble mean LINOZ  $4xCO_2$  ozone response with that from the OMA simulation (Figure  
 303 4). The amplitude and pattern of the ozone response in the LINOZ ensemble (Fig. 4b) is generally  
 304 very similar to the ozone response in the OMA simulation (Fig. 4a), consistent with Meraner et al.  
 305 (2020) who showed that the response of ozone to a quadrupling of  $CO_2$  is well captured using  
 306 linearized schemes. In both OMA and LINOZ configurations the pattern of the  $4xCO_2$  changes  
 307 reflects a decrease in tropical LS ozone, associated with enhanced tropical upwelling (Garcia and  
 308 Randel (2008)), and enhanced concentrations over high latitudes. Over all latitudes the ozone  
 309 changes are statistically significant, relative to interannual variability in the preindustrial control  
 310 simulation.

317 Over northern high latitudes there are some differences in the mid-to-lower stratosphere ( $\sim 30$ -100  
318 hPa) between LINOZ and OMA, generally consistent with Chiodo et al. (2018), who found that  
319 in this region the ozone response to  $\text{CO}_2$  is more dependent on (nonlinear) chemical and transport  
320 feedbacks and thus more likely to be captured using a more comprehensive chemistry scheme.  
321 Furthermore, both simulations feature small changes in the troposphere. Overall, therefore, the  
322 LINOZ scheme captures the gross characteristics of the ozone abrupt  $4\times\text{CO}_2$  response expected  
323 from previous studies. Note that most of this ozone response occurs in both simulations within the  
324 5-20 years that comprise the “fast” response timescale, as shown in Chiodo et al. (2018) (see their  
325 Figure 7b), although full equilibration at high latitudes does take somewhat longer (not shown).

326 In response to the ozone changes to  $4\times\text{CO}_2$  both the OMA simulation and LINOZ ensemble  
327 produce cooling in the tropical lower stratosphere and warming over high latitudes (Fig. 4c,d). The  
328 amplitude of the cooling is  $\sim 3\text{K}$  in the tropical lower stratosphere, and is more-or-less collocated  
329 with the region of largest ozone decreases. Further analysis of the temperature tendencies reveals  
330 that in our model the cooler temperatures in the tropics ( $20^\circ\text{S}$ - $20^\circ\text{N}$ ) and high latitudes ( $> 40^\circ\text{N}$ )  
331 are respectively associated with reduced and increased radiative heating, primarily in the shortwave  
332 component (not shown). Dynamically, comparisons of the  $4\times\text{CO}_2$  changes in the residual mean  
333 stream function show a weaker response in LINOZ, relative to NINT (not shown). This ozone  
334 feedback on the Brewer-Dobson circulation, first identified in DallaSanta et al. (2021a), contributes  
335 to reduced upwelling, adiabatic cooling, and ozone transport within the lower tropical stratosphere.  
336 These circulation changes are therefore not the primary drivers of the temperature response; rather,  
337 they are primarily determined by the shortwave radiative response to ozone changes (CP2019).

338 Despite the somewhat stronger cooling in OMA (Fig. 4c) compared to NINT (Fig. 4d), the  
339 temperature response in both configurations is within the 2-4 K range documented in CP2019 (note  
340 that all colorbars used are consistent with that study to facilitate comparisons with their results).  
341 An important point to note is that the temperature changes due to ozone are of a similar magnitude  
342 to the temperature changes due to  $4\times\text{CO}_2$  alone in the tropical lower stratosphere (i.e., considering  
343 no ozone feedback), where the stratosphere cools by  $\sim 2\text{K}$  in the NINT ensemble (not shown). The  
344 ozone changes present in LINOZ (and OMA) therefore represent a substantial ( $\sim 50\%$ ) feedback  
345 on the  $\text{CO}_2$ -induced cooling in the stratosphere at this altitude.

346 *c. Ozone Feedback on Northern Hemisphere Midlatitude Jet: Fast Response*

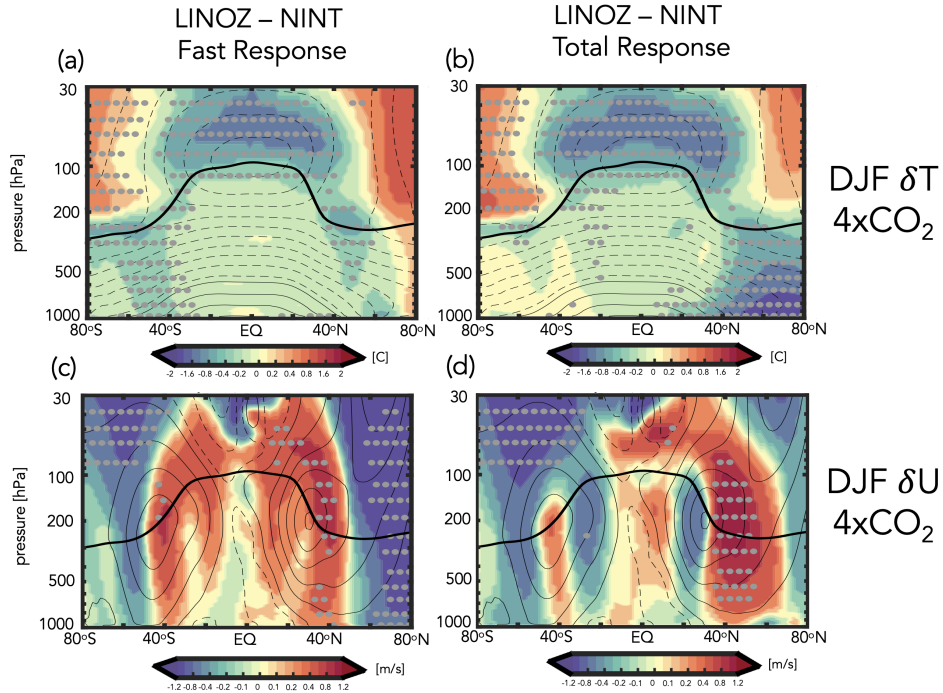
347 The temperature response due to ozone is dynamically consequential for the troposphere to the  
348 extent that it modifies temperature gradients (and winds) in the lower stratosphere. Indeed, the  
349 LINOZ ensemble shows a strong enhancement of lower stratospheric temperature gradients in both  
350 hemispheres on both the fast and total response timescales (Fig. 5a,b). In the fast response, this  
351 reduction in the meridional temperature gradient near the tropopause has important consequences  
352 for the midlatitude jet in both hemispheres, particularly in the NH where it strengthens above and  
353 along the jet core and weakens on the poleward flank of the jet over latitudes north of  $\sim 50^\circ\text{N}$  (Fig.  
354 5c). The winds also accelerate equatorward of the jet core, relative to NINT, in both hemispheres,  
355 although the response is only statistically significant in our model in the NH. This ozone-induced  
356 response in the jet is very similar to the pattern of the wind response reported in CP2019 (see  
357 their Figures 4 and 5). As with the temperature changes occurring in the lower stratosphere, the  
358 wind response to ozone changes is similar in magnitude to the  $4\times\text{CO}_2$  response, again suggesting  
359 a substantial modulation of the circulation in both hemispheres by ozone changes alone.

366 The fast zonal mean response to ozone changes reflects a weakening of the midlatitude jet over  
367 all longitudes, with the largest negative anomalies concentrated over the Atlantic ocean which are  
368 flanked equatorward by positive wind anomalies (Fig. 6a). This LINOZ-NINT wind dipole at  
369 850 hPa is very similar to the fast wind response captured in the fully interactive OMA simulation  
370 (Fig. 3c), especially over the Atlantic. This consistency with the response in OMA is also reflected  
371 at 300 hPa, where in both LINOZ and OMA configurations the winds accelerate between the  
372 climatological subtropical and midlatitude eddy-driven jets (Fig. A2c).

373 Over the Pacific, by comparison, the OMA and LINOZ responses are different, consistent with  
374 CP2019 who also found no robust ozone feedback over that sector (see their Figure 5). This lack  
375 of a robust ozone feedback over the Pacific is generally consistent with previous modeling and  
376 observational studies showing a much stronger signal of “downward” stratosphere-troposphere  
377 coupling over the Atlantic, relative to the Pacific (see Baldwin et al. (2021) and references therein),  
378 although this difference between sectors remains speculative and warrants closer inspection beyond  
379 the scope of the present study.

380 In addition to the near surface wind changes, the weakening of the North Atlantic jet in the  
381 LINOZ simulations is associated with warming over North America and cooling over the North



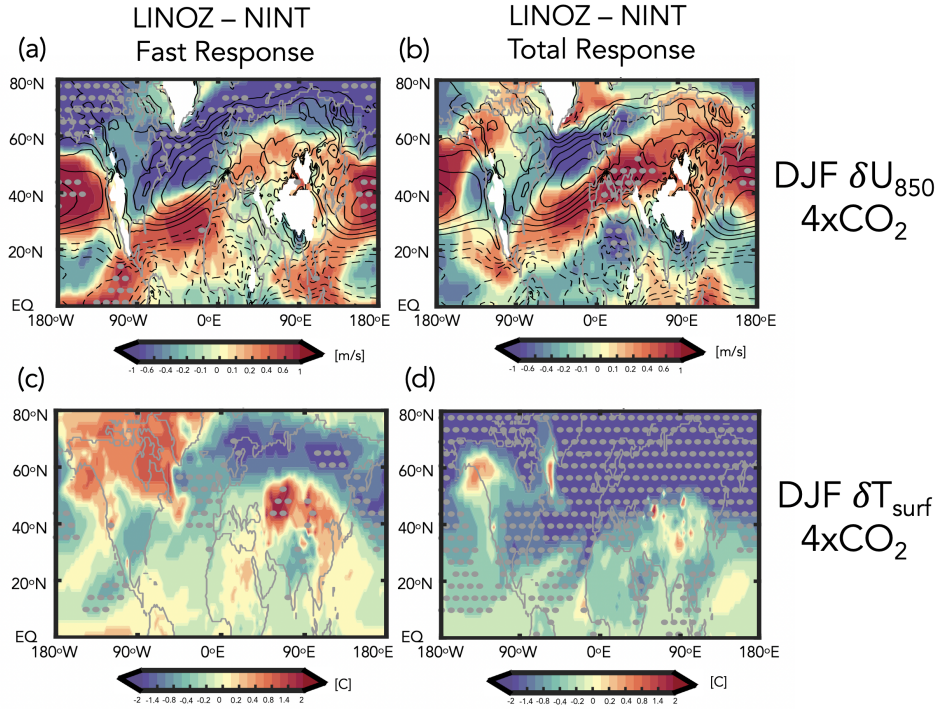


360 FIG. 5. Colors show the LINOZ-NINT ensemble mean difference in the DJF response of the zonal mean  
 361 temperatures,  $T$  (top) and zonal winds,  $U$  (bottom) in response to an abrupt quadrupling of  $\text{CO}_2$ . Both LINOZ  
 362 and NINT ensembles consist of four members. Responses are decomposed into “fast” (a,c) and “total” (b,d)  
 363 changes. Contours denote climatological mean DJF values ( $T$  contour interval: 10 C;  $U$  contour interval: 8 m/s).  
 364 Stippled regions are statistically significant and the black thick line shows the climatological mean tropopause in  
 365 the preindustrial control simulation.

382 Atlantic and over Eurasia, resembling the negative phase of the NAO (Fig. 6c). A similar surface  
 383 temperature anomaly was identified in CP2019 (see their Figure 7) and in our model occur in  
 384 conjunction with positive sea level pressure (SLP) anomalies over the Arctic (Appendix Figure A3,  
 385 top), both features being reminiscent of a negative NAO.

390 *d. Ozone Feedback on Northern Hemisphere Midlatitude Jet: Total Response*

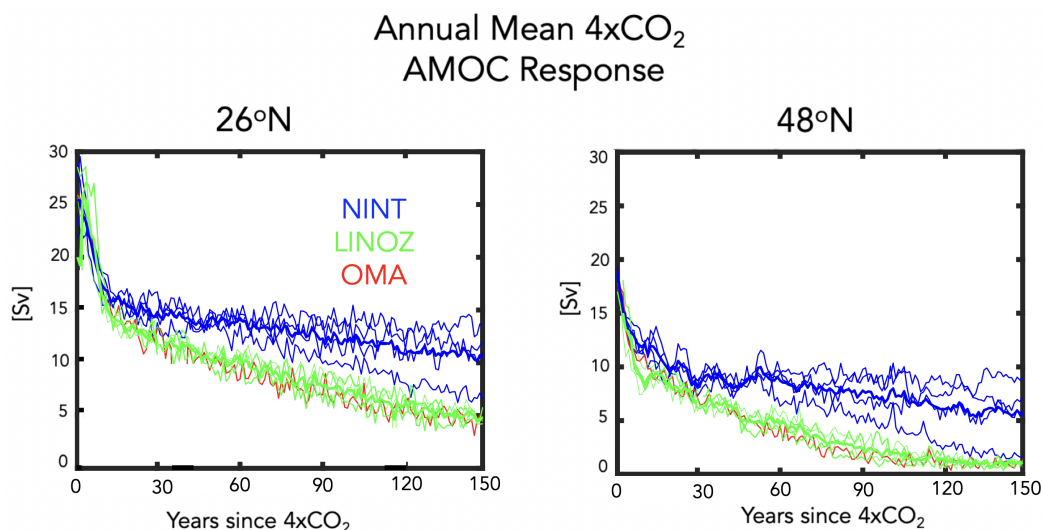
391 Interestingly, while the fast responses in the winds and temperatures in the LINOZ ensemble are  
 392 highly consistent with the results from CP2019, our model also simulates a distinct “total” response  
 393 characterized by strong cooling over the Arctic from the surface to the mid-to-upper troposphere  
 394 (Fig. 5b). This cooling, which was not identified in CP2019, results in enhanced mid-to-lower



386 FIG. 6. Same as Figure 5, except showing the LINOZ-NINT DJF response in the 850 hPa zonal winds,  $U_{850}$   
 387 (top) and surface temperatures,  $T_{\text{surf}}$  (bottom). Contours in top panels denote climatological mean DJF values  
 388 of  $U_{850}$  (contour interval: 2 m/s). Note the similarity between the “fast” wind response shown in (a) and the  
 389 CP2019 results (their Figure 6).

395 tropospheric temperature gradients, prompting a strong poleward shift of the zonal mean NH jet  
 396 and a statistically significant acceleration of the winds at  $50^{\circ}\text{N}$  exceeding 2 m/s (Fig. 5d).

397 Zonally, the cooling over the Arctic occurring in the LINOZ ensemble during the total response  
 398 primarily reflects hemispheric-wide cooling over the Arctic associated with an expansion of the  
 399 North Atlantic Warming Hole (Fig. 6d). This enhancement of meridional temperature gradients  
 400 in the lower and mid troposphere drives a poleward shift that spans all longitudes and originates  
 401 over the North Atlantic (Fig. 6b), where the jet exhibits a distinct acceleration and eastward  
 402 extension over Europe. Note that over the jet core ( $40^{\circ}\text{N}$ - $50^{\circ}\text{N}$ ) the winds accelerate (in the zonal  
 403 mean) during both “fast” (Fig. 5c) and “total” responses (Fig. 5d). However, north of  $50^{\circ}\text{N}$  the  
 404 responses are very different, with the fast response exhibiting a strong weakening, in contrast to  
 405 the acceleration occurring on longer (i.e., “total” response) timescales. This behavior north of  $50^{\circ}\text{N}$



420 FIG. 7. Evolution of the annual mean maximum overturning stream function in the Atlantic ocean, evaluated  
 421 at  $26^\circ N$  (left) and  $48^\circ N$  (right) in response to  $4xCO_2$ . Results for the LINOZ and NINT ensembles are shown  
 422 in green and blue, respectively (thick lines denote ensemble means). Red lines show the response in the OMA  
 423 simulation.

406 was not captured in CP2019 and comprises a coupled ozone-ocean feedback that is distinct from  
 407 what was outlined in that study.

#### 408 *e. Total Ozone Feedback: Modulation by the AMOC*

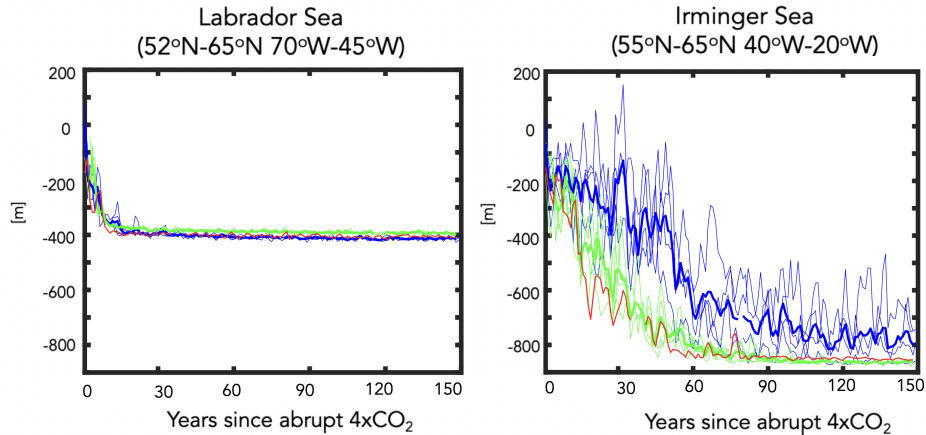
409 The “total” responses in the tropospheric winds and temperatures that occur in the LINOZ  
 410 ensemble are not obviously linked to ozone-driven temperature changes in the stratosphere, which  
 411 do not extend into the troposphere. What, then, is the driver of the lower tropospheric high latitude  
 412 cooling, if it is not directly linked to ozone-driven stratospheric temperature changes?

413 As expected from the OMA and NINT results presented in Zhang et al. (2023) and summarized  
 414 in Figure 2, we find that the strong cooling that occurs over the NH in the total LINOZ response is  
 415 also related to a weakening of the AMOC at  $4xCO_2$  (Mitevski et al. (2021); Orbe et al. (2023)). In  
 416 particular, Figure 7 shows stronger weakening of the AMOC in the LINOZ (green lines) ensemble,  
 417 relative to NINT (blue lines) at both  $26^\circ N$  (left) and at  $48^\circ N$  (right). Despite large internal  
 418 variability, the LINOZ ensemble shows a more rapid decline of the AMOC, a difference that is  
 419 evident at both latitudes.

424 Interestingly, comparisons of the AMOC behavior in LINOZ with the fully interactive OMA  
425 simulation (red line) shows a striking similarity (and the mechanism of these changes is also similar,  
426 as shown in Section 3f). This similarity is surprising, given that other (non-ozone) trace gases and  
427 aerosols are also evolving in the OMA experiment. In particular, Rind et al. (2018), using a previous  
428 version of the model, observed an indirect effect of natural aerosols (primarily sea salt) on AMOC  
429 stability. They showed that aerosols enhanced the local cooling of SSTs in regions of increased  
430 cloud cover in a warmer climate by acting as condensation nuclei and thereby raising cloud optical  
431 thickness and ocean surface cooling. This surface cooling was then linked to reduced evaporation  
432 relative to precipitation, resulting in anomalously positive surface freshwater forcing and reduced  
433 North Atlantic Deep Water (NADW) production. That study, however, focused on aerosol-induced  
434 AMOC cessations occurring on multicentennial timescales long after the initial (abrupt) warming.  
435 By comparison, the results in Figure 7 identify an impact of ozone on the AMOC that occurs within  
436 the first 20 years of the initial CO<sub>2</sub> forcing – that is, over the period during which ozone is also  
437 rapidly evolving (Chiodo et al. 2018) and stratospheric temperature gradients are most impacted  
438 by changes in ozone (not aerosols). Our results, therefore, highlight that during this time frame the  
439 AMOC can be as (if not more) sensitive to wind-driven buoyancy changes forced by stratospheric  
440 ozone anomalies as they are to aerosol-induced changes in freshwater forcing.

441 Before elucidating the mechanism of the AMOC changes in the LINOZ ensemble, we first  
442 identify the region over which the largest differences in mixed layer depth begin to emerge between  
443 the LINOZ (OMA) and NINT simulations. In particular, the weaker AMOC in the LINOZ and  
444 OMA runs is found to be accompanied by a rapid reduction in mixed layer depths, which occur  
445 primarily in the Irminger Sea region (55°N-65°N, 40°W-20°W) (Figure 8). The mixed layer depth  
446 differences among the configurations in the Labrador Sea are, by comparison, negligible. East of  
447 the Irminger Sea (i.e., 55°N–65°N, 20°W-0°) we also identify differences between the ensembles  
448 (not shown), but these emerge later, suggesting that the Irminger Sea changes are likely the initiators  
449 of the differences in AMOC behavior between the NINT and LINOZ ensembles. The same region  
450 was identified in Romanou et al. (2023) as being key for determining the sensitivity of the AMOC in  
451 various SSP 2-4.5 ensemble runs, albeit for simulations conducted using the low-top GISS climate  
452 model.

## DJF 4xCO<sub>2</sub> Response in Mixed Layer Depth



453 FIG. 8. Changes in the DJF mixed layer depths, evaluated over the Labrador Sea (left) and Irminger Sea  
 454 (right) in response to 4xCO<sub>2</sub>, relative to the preindustrial control simulations. Results for the LINOZ and NINT  
 455 ensembles are shown in green and blue, respectively (thick lines denote ensemble means). Red lines show the  
 456 response in the OMA simulation.

### 457 *f. Ozone Feedback Dependence on the AMOC: Linking Fast and Total Responses*

458 Is the fact that the AMOC declines more rapidly in the LINOZ ensemble – and the OMA  
 459 simulation – a response to the ozone changes in those simulations or just a coincidence? In the fast  
 460 response the zonal wind changes over the North Atlantic reflect a weakening of the jet core that is  
 461 flanked equatorward by positive anomalies, resembling a negative NAO pattern. Indeed, a negative  
 462 (positive) NAO has been associated with a weaker (stronger) AMOC by adding (extracting) heat  
 463 to/from the subpolar gyre, resulting in reduced (increased) NADW formation (Delworth and Zeng  
 464 (2016)). Here we argue that such a mechanism is present in our model simulations, resulting in a  
 465 long-term modulation of the NH midlatitude jet by ozone that occurs indirectly through changes  
 466 in the AMOC.

467 In particular, Figure 9 shows maps of the surface zonal wind, surface friction speed, mixed layer  
 468 depth, net heat fluxes, sea surface temperatures, and north-south heat and salinity ocean transports,  
 469 averaged over years 1-5. In response to an abrupt quadrupling of CO<sub>2</sub>, the surface winds weaken  
 470 over the subpolar North Atlantic region in NINT, leading to a weak acceleration of the zonal winds

471 on the poleward flank of the North Atlantic jet ( $\sim 60^\circ\text{N}$ - $70^\circ\text{N}$ ) (Fig. 9a, top). Over the subpolar  
472 North Atlantic the weakening of the surface winds leads to a significant reduction in surface friction  
473 speed (Fig. 9b, top) and mixed layer depths (Fig. 9c, top), as well as increased heat flux into  
474 the ocean (in the form of reduced latent heat fluxes out of the ocean) (Fig. 9d, top) and warmer  
475 sea surface temperatures (Fig. 9e, top). The reduced surface density during the first 20 years  
476 associated with these warmer temperatures lead to a rapid decrease in mixed layer depth by some  
477 200 m (Figure 8) and the overturning circulation by  $\sim 40\%$  (Figure 7) in NINT. At these early years  
478 the changes in meridional heat and salinity transports over the Irminger Sea are relatively small  
479 (Fig. 9fg, top).

480 However, in response to the ozone changes captured in the LINOZ ensemble during years 1-5,  
481 there is an even stronger reduction in the surface zonal winds and friction speed (Fig. 9 ab, bottom),  
482 consistent with the negative NAO response evident in the 850 hPa zonal winds (Fig. 6c, top). The  
483 surface friction changes align closely with the reduced mixed layer depths which extend well into  
484 the Irminger Sea region and over latitudes further south of the subpolar gyre (Fig. 9c, bottom).

485 The reductions in mixed layer depth that occur over the Irminger Sea are likely driven by the  
486 reductions in surface wind speed which increase (primarily latent) heat fluxes into the ocean (Fig.  
487 9d, bottom), driving warmer sea surface temperatures in LINOZ, relative to NINT (Fig. 9e,  
488 bottom). The sign of the response of the heat fluxes in the subpolar gyre region is consistent with  
489 previous studies showing that a positive (negative) phase of the NAO implies reduced (enhanced)  
490 atmosphere to ocean heat fluxes (Delworth et al. (2017)). Furthermore, the spatial pattern of  
491 the heat flux response is very similar to the NAO heat flux composites that were prescribed in  
492 Delworth and Zeng (2016) and inferred from observations in Ma et al. (2020) (see their Figure  
493 6), who showed that there is much greater heat loss from the ocean over the subpolar region in  
494 association with a jet strengthening.

495 At the same time, the changes in freshwater forcing (P-E) during this time period are negligible  
496 such that the net buoyancy forcing comprising the sum of both net heat and freshwater fluxes ( $\sim Q+F$ )  
497 is positive. This stabilizing buoyancy forcing from surface warming makes the mixed layer depths  
498 shallower by suppressing convective mixing, shutting down NADW production (Alexander et al.  
499 (2000); Kantha and Clayson (2000)). There is also an initial change in the north-south heat and  
500 salt transports that is colocated with the dipole anomaly in the surface friction speed, promoting

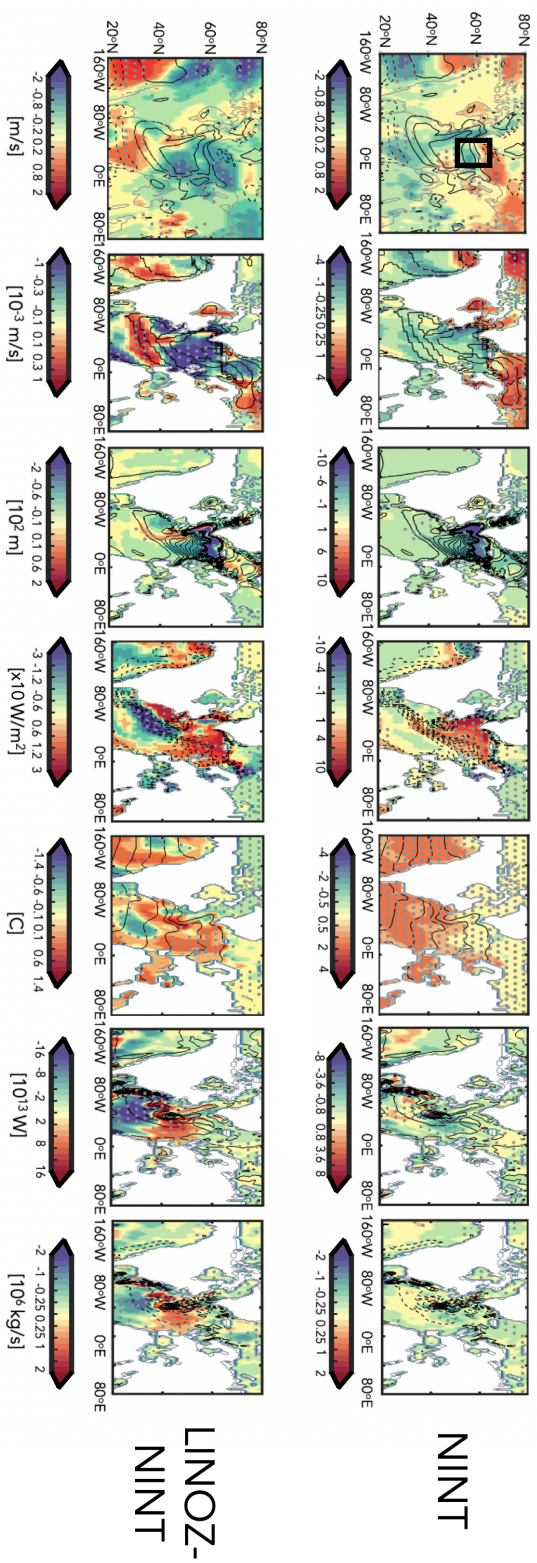
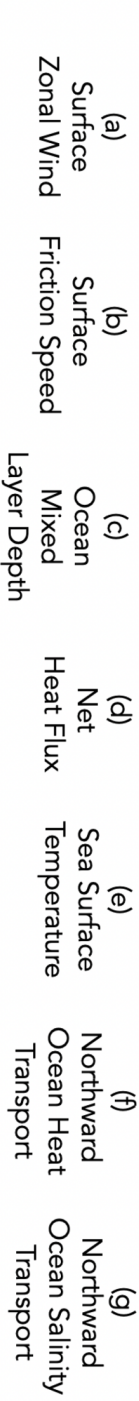
501 anomalous poleward salt and heat transport into the subpolar gyre (Fig. 9fg, bottom). This feature  
502 is confined to the top few ocean layers (not shown) and the implied anomalous heat transport could  
503 be contributing to the warmer sea surface temperatures in that region, in addition to the surface  
504 heat flux changes.

513 Over the ensuing years (5-20) a similar pattern is maintained in the LINOZ ensemble (Figure  
514 10, middle row). The reduction in NADW, however, results in reduced northward heat and salinity  
515 transports (Fig. 10 fg, middle) throughout the ocean column. While this results in cooler SSTs  
516 south of the subpolar gyre region (Fig. 10e, middle), which otherwise might enhance the density  
517 of the near-surface water masses, the reduced northward salinity transports prevent the AMOC  
518 from restarting. Interestingly, the results from the OMA simulation show a very similar response  
519 as the LINOZ ensemble (Figure 10, bottom row), suggesting that stratospheric ozone changes in  
520 that simulation are also likely the primary driver of the weaker AMOC in that model configuration.  
521 This sequence of processes linking the surface wind changes to anomalous heat fluxes and reduced  
522 NADW is basically identical to what is outlined in Figure 4 of Delworth and Zeng (2016) and  
523 Figure 1 of Khatri et al. (2022). Additional analysis of the 2xCO<sub>2</sub> simulations, which feature a  
524 stronger AMOC decline in OMA (and LINOZ) compared to NINT (Figure 2), reveals that a similar  
525 mechanism for reduced NADW production occurs at lower CO<sub>2</sub> forcing (not shown).

529 Examining the timescale of the responses of the variables shown in Figures 9 and 10 reinforces  
530 the strong coupling between the changes in surface friction speed, sea surface temperature, latent  
531 heat fluxes and mixed layer depth changes over the Irminger Sea region (Figure 11a-d). Despite  
532 large internal variability, there is a clear separation between the LINOZ (and OMA) and NINT  
533 ensembles that emerges around year 15 (black dashed lines). The changes in sensible heat emerge  
534 after the latent heat fluxes (Fig. 11e), suggesting that the latter play a more important role in  
535 initializing the heat flux differences in LINOZ (and OMA), relative to NINT.

536 Finally, while they may contribute to enhanced positive buoyancy forcing later in the integrations,  
537 the freshwater forcing anomalies ( $F = P - E$ ) are shown to be negligible during the initial years  
538 following the abrupt quadrupling of CO<sub>2</sub> (Fig. 11f), indicating that the primary driver of the  
539 initial difference between the LINOZ (and OMA) and NINT runs is related to the surface wind-  
540 driven changes as they impact the latent heat fluxes into the ocean. This is consistent with Roach  
541 et al. (2022) who showed a much stronger correlation between AMOC strength at 26°N and the

# DJF 4xCO<sub>2</sub> Response over Years 1-5



505 Fig. 9. Top panels: Colors show the December-January-February (DJF) response of the surface zonal wind (a), surface friction speed (b), ocean  
 506 mixed layer depth (c), net heat flux (sum of sensible plus latent heat) (d), sea surface temperature (e) and northward heat (f) and salt (g) transports in  
 507 response to an abrupt quadrupling of CO<sub>2</sub>. Results are shown for the 4-member ensemble averaged NINT configuration. Bottom panels: Same as top  
 508 panels, except showing the LINOZ minus NINT ensemble mean difference. For both top and bottom panels, responses have been averaged over years  
 509 1-5 since “branching” from the preindustrial control simulation. Stippled regions are statistically significant and black contours denote climatological  
 510 mean preindustrial control DJF values. Contour intervals: surface zonal wind [2 m/s], surface friction speed [2.5x10<sup>-3</sup> m/s], mixed layer depth [60 m],  
 511 net heat flux [30 W/m<sup>2</sup>], sea surface temperature interval [2 C], northward heat flux [2x10<sup>12</sup> W], and northward salt flux [10<sup>6</sup> kg/s]. The black box in  
 512 (a) bounds the Irminger Sea region over which the spatial averages in Figure 8b and Figure 11 are evaluated.



# DJF 4xCO<sub>2</sub> Response over Years 5-20

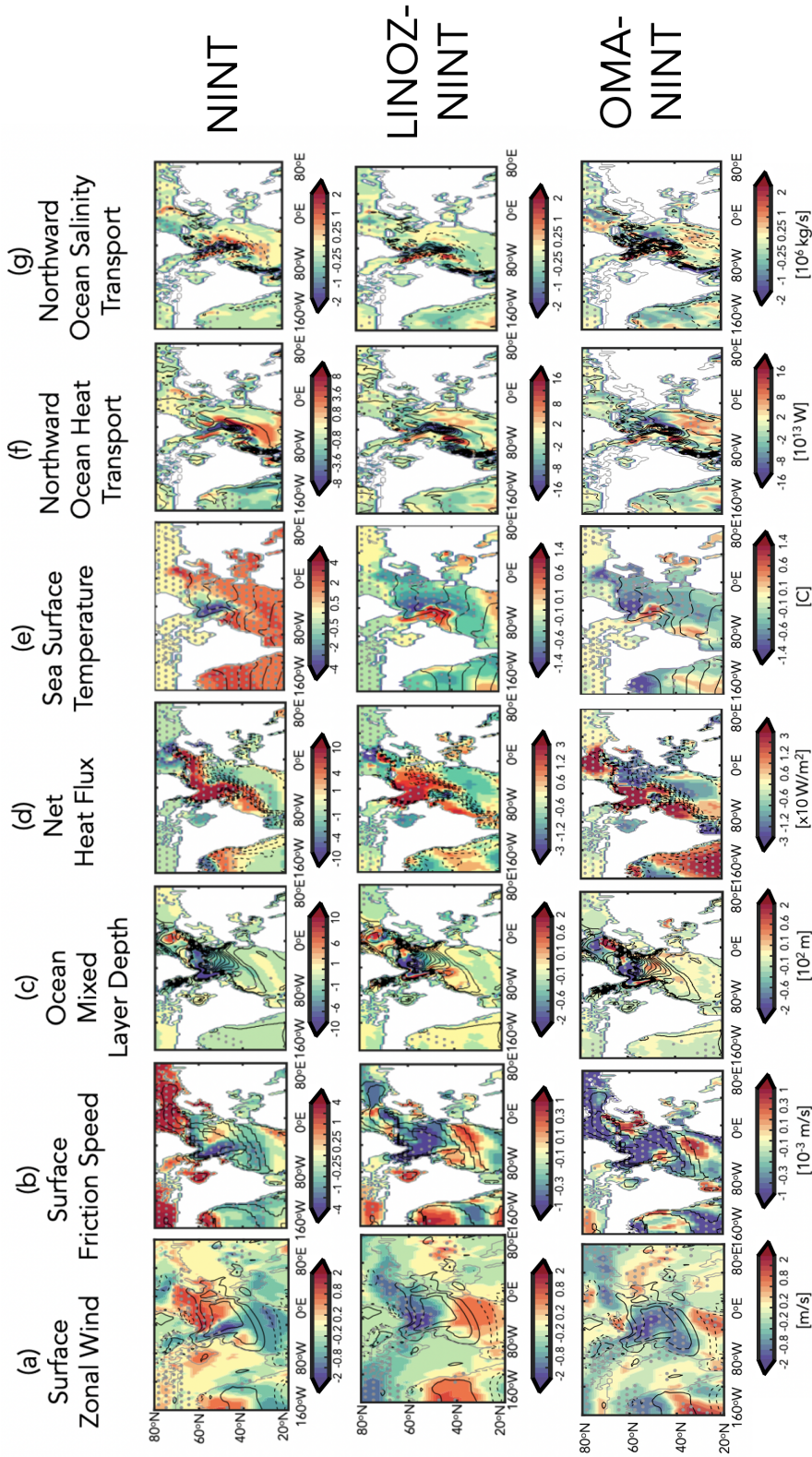


Fig. 10. Same as Figure 9, except showing the responses, averaged over years 5-20. An extra row at the bottom has been added, showing the OMA-NINT differences, where the ensemble members shown in Figures 1, 2 and 3 have been used. Same contour intervals and colorbars have been used as in Fig. 9.

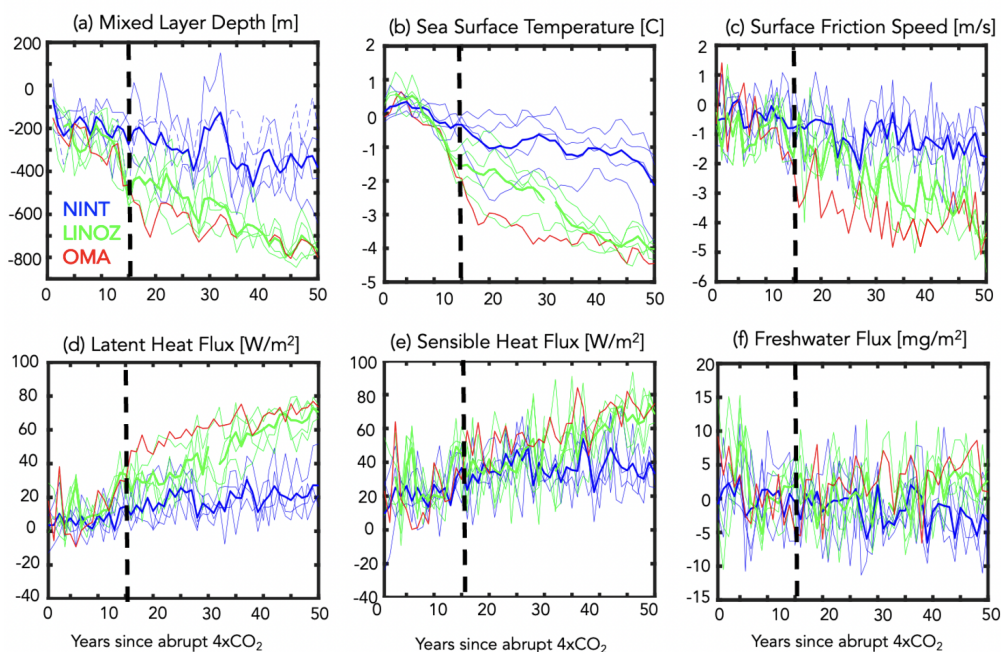
542 heat component of the surface buoyancy flux, relative to the freshwater component, in various  
543 experiments using the Community Earth System Model version 1 (CESM1) in which the winds  
544 over the subpolar gyre were nudged to reanalysis values. Note that in our model other potential  
545 contributors to freshwater forcing from sea ice do reveal differences between the LINOZ, OMA  
546 and NINT ensembles, but these emerge several years (i.e., years ~20-30) after the changes in sea  
547 surface temperatures and heat fluxes (not shown).

558 *g. Ozone Driver of AMOC Changes: Fixed SST and SIC Results*

559 So far, we have shown that the stratospheric ozone changes that occur in response to  $4\times\text{CO}_2$   
560 result in a negative NAO response over the North Atlantic (Fig. 5,6). In our model this triggers a  
561 more rapid decline of the AMOC (Fig. 7) through surface-wind driven changes in heat fluxes into  
562 the ocean (Fig. 9,10). While the time series analysis (Fig. 11) reveals that the AMOC changes  
563 in the LINOZ (OMA) ensemble occur on similar timescales as the wind (and heat flux) changes,  
564 one potentially confounding factor is the fact that the AMOC reduction itself results in reduced  
565 wind speeds over the subpolar gyre region. These reduced near-surface winds are associated with  
566 an anomalous anticyclonic flow pattern (Fig. A3, top; also discussed in Gervais et al. (2019);  
567 Romanou et al. (2023); Orbe et al. (2023)), which could contribute to the reduced heat fluxes and  
568 subsequent changes in NADW production. Therefore, to more convincingly link the surface wind  
569 speed changes to the stratospheric ozone changes aloft, we next examine results from the fixed  
570 preindustrial control SST and SIC experiments.

571 Figure 12 shows the ozone-induced zonal wind and temperature changes averaged over the last  
572 twenty years of the fixed preindustrial control SST and SIC experiments in which the time-varying  
573 zonally varying ozone from the  $4\times\text{CO}_2$  LINOZ ensemble is prescribed (Fig. 12 a,b). Recall that in  
574 the fixed SST and SIC experiments, only the ozone evolution differs from the preindustrial control  
575 simulation, as  $\text{CO}_2$ , SSTs and SIC are all set to preindustrial values. Comparisons with results  
576 from the fully coupled LINOZ “fast” response (see Fig. 5a,c) reveal a very similar picture. This  
577 similarity between the fully coupled fast response and the fixed preindustrial control SST and SIC  
578 experiments is striking, both featuring a similar change in the NH jet associated with enhanced  
579 temperature gradients in the lower stratosphere as first reported in CP2019.

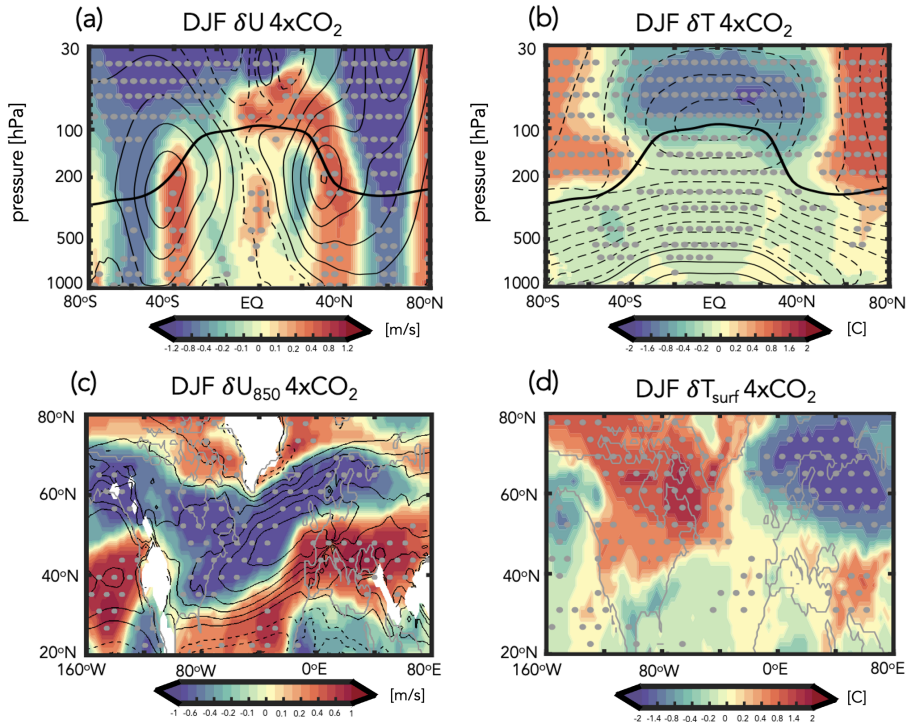
## DJF 4xCO<sub>2</sub> Response over Irminger Sea



548 FIG. 11. Changes in the DJF mixed layer depths (a), sea surface temperatures (b), surface friction speed (c),  
 549 latent heat fluxes (d), sensible heat fluxes (e) and precipitation minus evaporation (f) in response to 4xCO<sub>2</sub>,  
 550 relative to the preindustrial control simulations. Averages are performed over the Irminger Sea (55°N-65°N,  
 551 40°W-20°W) and the x-axis is restricted to years 1-50 in order to highlight the fast timescales on which the mixed  
 552 layer depths, surface friction speed and heat fluxes evolve together. Results for the LINOZ and NINT ensembles  
 553 are shown in green and blue, respectively (thick lines denote ensemble means). Red lines show the response in  
 554 the OMA simulation. Black vertical lines indicate year ~15 at which point the mixed layer depth responses in  
 555 the LINOZ and NINT ensembles diverge. Note that the freshwater flux unit of 1 mg/m<sup>2</sup> per second ( $\equiv 0.0864$   
 556 mm/day  $\equiv 3.1$  cm/year) is used, because at 5°C it contributes approximately the same ocean density flux as the  
 557 heat flux unit of 1 W/m<sup>2</sup> (Large and Yeager (2009)).

580 Comparisons of the 850 hPa zonal winds and surface temperatures over the North Atlantic  
 581 (Fig. 12c,d) also reveal a strikingly similar response between the fully coupled ensemble and the  
 582 fixed preindustrial control SST and SIC experiments (compare with Fig. 6a,c). Over the Atlantic  
 583 this similarity also holds aloft in the zonal wind response at 300 hPa (Fig. A2e) and in the sea  
 584 level pressure response (Fig. A3, bottom). The consistency in the sea level pressure changes is

## LINOZ – NINT Fixed SST Changes



590 FIG. 12. Top panels: Colors show the 4xCO<sub>2</sub> ensemble mean response in zonal mean zonal winds, U (a),  
 591 temperatures, T (b), 850 hPa zonal winds, U<sub>850</sub> (c) and surface temperature, T<sub>surf</sub> (d) in the prescribed SST and  
 592 SIC experiments in which the time-evolving 4xCO<sub>2</sub> ensemble mean LINOZ ozone response is prescribed. Note  
 593 that SSTs, SICs and background CO<sub>2</sub> are all set to preindustrial values. Averages are shown over the last 20 years  
 594 (years 40-60) of the integrations. Black contours, where shown, denote climatological mean preindustrial control  
 595 DJF values (U contour interval: 8 m/s; T contour interval: 10 C; U<sub>850</sub> contour interval: 2 m/s). Stippled regions  
 596 are statistically significant and the black thick line in the top panels shows the climatological mean tropopause in  
 597 the preindustrial control simulation.

585 interesting as it suggests that over the North Atlantic stratospheric ozone changes alone can result  
 586 in a significant reduction in the near surface winds that is on the same order (if not larger than)  
 587 the 4xCO<sub>2</sub> response. In our coupled atmosphere-ocean model this additionally results in heat  
 588 flux changes that are large enough to reduce NADW production, resulting in a significant (i.e.  
 589 ~30-40%) long-term change in AMOC strength.

## 598 4. Conclusions

599 Here we have used the NASA GISS coupled atmosphere-ocean high-top model (E2.2-G) to  
600 examine how coupled changes in stratospheric ozone and the ocean circulation both influence the  
601 abrupt  $4\times\text{CO}_2$  response of the NH midlatitude jet. Our key results are as follows:

- 602 • The NH midlatitude jet response to  $4\times\text{CO}_2$  is modulated by coupled feedbacks from both  
603 stratospheric ozone and the AMOC, which occur on “fast” (5-20 year) and “total” (100-150  
604 year) timescales, respectively.
- 605 • In the “fast” response, the zonal mean jet weakens (strengthens) on its poleward (equatorward)  
606 flank, consistent with reduced LS temperature gradients associated with ozone loss in the  
607 tropics. Zonally, this jet change is expressed as a negative NAO-like pattern, consisting of  
608 weaker zonal surface winds over the North Atlantic, consistent with the findings in CP2019.
- 609 • The weaker winds over the North Atlantic are associated with increased (primarily latent) heat  
610 fluxes into the ocean, which initially result in warmer SSTs over the subpolar gyre region,  
611 reducing NADW production and leading to more rapid weakening of the AMOC.
- 612 • A reduced AMOC leads to widespread cooling over the Arctic which enhance mid-to-lower  
613 tropospheric temperature gradients, resulting in a poleward shift of the NH midlatitude jet.  
614 This “total” response is consistent with previous studies showing that a weakening of the  
615 AMOC results in a stronger and poleward shifted jet in the NH (e.g., Bellomo et al. (2021);  
616 Orbe et al. (2023); Liu et al. (2020); Zhang et al. (2023)).

617 Taken together, the findings listed above indicate that the stratospheric ozone feedback on the NH  
618 midlatitude jet reported in CP2019 is coupled to the behavior of the AMOC during the “fast”  
619 response, wherein the jet weakens over the North Atlantic. In our model, this wind response  
620 extends to the surface, resulting in reduced heat fluxes out of the subpolar gyre region and a more  
621 rapid decline of the AMOC. On longer timescales, these changes in the AMOC subsequently  
622 drive a poleward shift in the NH midlatitude jet. Unlike the “fast” response, this “total” timescale  
623 response in the NH jet to changes in stratospheric ozone has not been previously reported, to the  
624 best of our knowledge. This may reflect differing sensitivities of the AMOC among models and  
625 our results will, of course, need to be tested using other models to assess robustness.

626 Another intriguing result from this study is that the stronger decline of the AMOC in the LINOZ  
627 ensemble does not appear to be a coincidence. Rather, in our model, the “fast” ozone and “total”  
628 AMOC feedbacks on the NH jet are coupled through surface-wind driven changes in heat fluxes  
629 into the ocean. Key here is the fact that this sensitivity in the AMOC is driven only by changes in  
630 stratospheric ozone, which we have isolated from changes in other trace gases and aerosols. Thus,  
631 while previous studies (Rind et al. (2018)) have identified an important influence of interactive  
632 composition on the AMOC, they have mainly implicated the indirect effect of aerosols on clouds  
633 through changes in sea surface temperatures and how these impact P-E (and net surface freshwater  
634 forcing). To the best of our knowledge, no study has previously demonstrated an impact of  
635 stratospheric ozone changes alone on the AMOC response to a quadrupling of CO<sub>2</sub>. Despite the  
636 different mechanisms at play, however, are results are generally consistent with those from Rind  
637 et al. (2018) in highlighting the need for renewed focus on surface flux observations to help assess  
638 overturning stability.

639 An important caveat with our results is related to known biases in vertical mixing and NADW  
640 production in the ocean component of the GISS model (Miller et al. (2021); Romanou et al.  
641 (2023)) which likely explain why the low-top version of the coupled atmosphere-ocean climate  
642 model (E2.1-G) exhibits a more sensitive AMOC response to a quadrupling of CO<sub>2</sub>, compared  
643 to some other models (Bellomo et al. (2021)). An important point to highlight, however, is that  
644 the high-top model employed in this study is much less sensitive, as the AMOC weakens by ~10  
645 SV in response to 4xCO<sub>2</sub>, compared to a complete collapse in E2.1-G (see Figure 31 in Rind  
646 et al. (2020)). That study showed that this may be related to differences in the parameterization of  
647 rainfall evaporation associated with moist convective precipitation, which they show has a strong  
648 influence on the AMOC sensitivity in the GISS model via its effect on moisture loading in the  
649 atmosphere. While an exhaustive comparison between the models is beyond the scope of this  
650 study, the relevant point here is that the 4xCO<sub>2</sub> AMOC response simulated in the E2.2-G NINT  
651 ensemble is well within the CMIP5 and CMIP6 ranges documented in Mitevski et al. (2021) (see  
652 their Supplementary Figure S3).

653 A natural next step for future research is to examine whether this influence from stratospheric  
654 ozone is evident in more realistic scenarios. Although not examined in equal depth, results from the  
655 more realistic 1%CO<sub>2</sub> transient simulations also show a greater weakening of the AMOC in OMA,

656 relative to NINT, indicating that the findings presented here are not an artifact of the abruptness  
657 of the forcing (not shown). Analysis of the more comprehensive historical and future Shared  
658 Socioeconomic Pathway (SSP) (Meinshausen et al. (2020)) integrations is currently underway to  
659 identify other factors, including aerosols and the solar cycle (Muthers et al. (2016)), which are  
660 likely to influence the ocean circulation. For sake of brevity, however, we reserve further discussion  
661 of the more comprehensive results for future work.

662 Finally, our results linking the fast timescale jet response to the ensuing AMOC changes un-  
663 derscore the profound impact that changes in lower stratospheric winds alone can have on surface  
664 climate, as highlighted in Sigmond and Scinocca (2010). Quite remarkably, our fixed SST and SIC  
665 experiments showed that these lower stratospheric wind changes are driven primarily by changes  
666 in ozone and not by background changes in CO<sub>2</sub> or in sea surface boundary conditions. Taken  
667 together, our results suggest that more attention needs to be paid to understanding the time-evolving  
668 response of the coupled Earth system to future ozone changes, with a focus on changes in ocean  
669 heat transport and how these feed back on the NH jet stream.

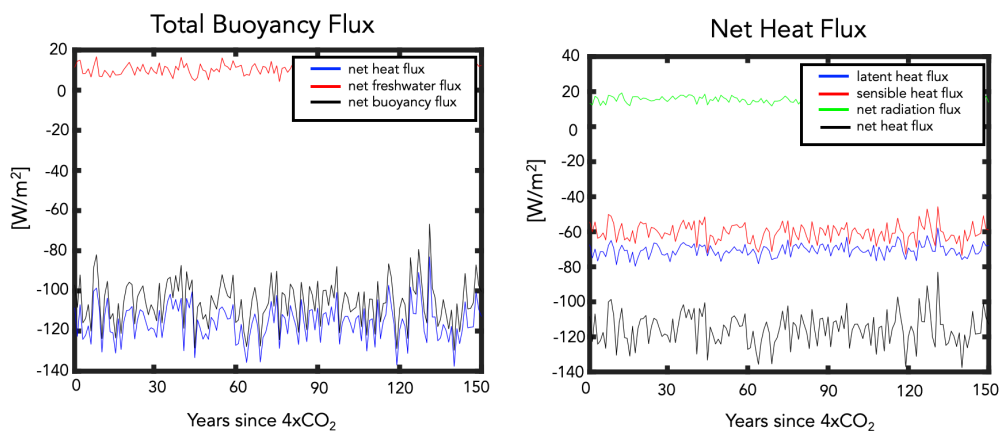
670 *Acknowledgments.* C.O. acknowledges helpful discussions with Lettie Roach, Ivan Mitevski  
671 and Lorenzo Polvani. G.C. acknowledges support by the SNSF with the “Ambizione” grant  
672 N. PZ00P2180043. Climate modeling at GISS is supported by the NASA Modeling, Analysis and  
673 Prediction program, and resources supporting this work were provided by the NASA High-End  
674 Computing (HEC) Program through the NASA Center for Climate Simulation (NCCS) at Goddard  
675 Space Flight Center.

676 *Data availability statement.* The NINT and OMA GISS E2.2-G simulations used in the study  
677 are available at the CMIP6 archive via the Earth System Grid Federation ([https://esgf-node.  
678 llnl.gov/](https://esgf-node.llnl.gov/)), where NINT and OMA are respectively denoted as “physics version 1” and “physics  
679 version 3”. The specific simulations used here are the PiControl, abrupt-2xCO<sub>2</sub>, and abrupt-  
680 4xCO<sub>2</sub> r1i1p1f1 (NINT) and r1i1p3f1 (OMA) runs. Output needed to reproduce all figures  
681 showing the additional three NINT 4xCO<sub>2</sub> simulations, fixed SST simulations as well the four-  
682 member LINOZ ensemble is available online at [https://gmao.gsfc.nasa.gov/gmaoftp/  
683 corbe/AMOC\\_Linoz/Data/](https://gmao.gsfc.nasa.gov/gmaoftp/corbe/AMOC_Linoz/Data/). All GISS ModelE components are open source and available at  
684 <http://www.giss.nasa.gov/tools/modelE/>.

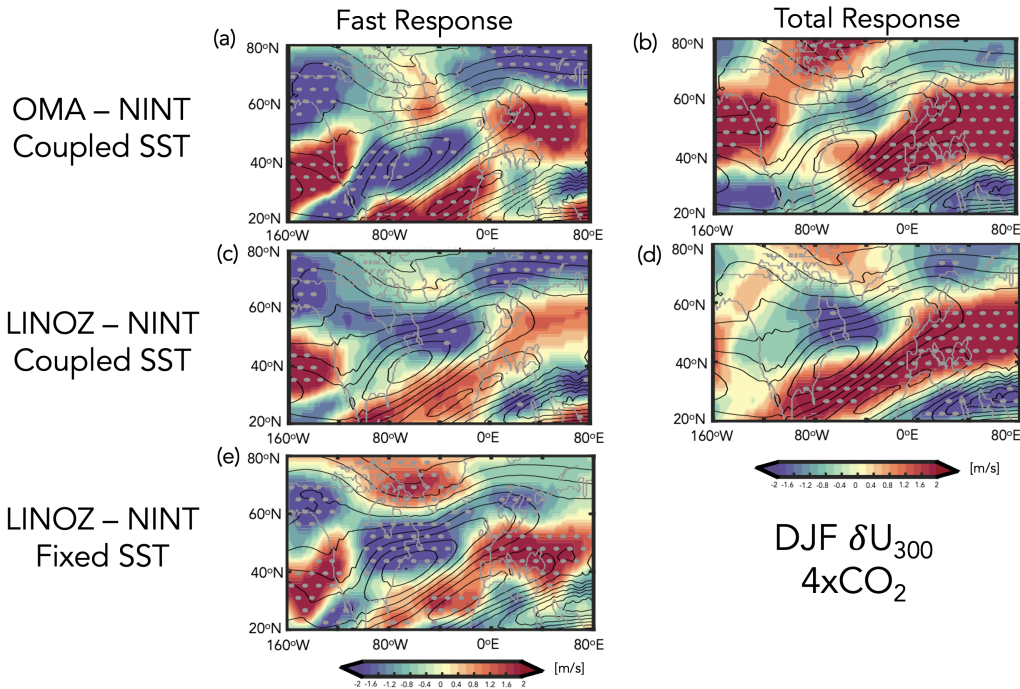
## 685 APPENDIX



Annual Mean PiControl Climatological  
Flux Decompositions over the Irminger Sea

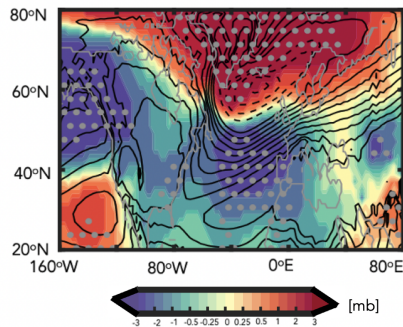


686 FIG. A1. Left: Decomposition of the net surface buoyancy flux (black) into contributions from net heat  
 687 (blue) and net freshwater (red) fluxes. Right: Further decomposition of the net surface heat flux (black) into  
 688 contributions from latent heat fluxes ( $Q_E$  (blue)), sensible heat fluxes ( $Q_H$  (red)), and combined solar and  
 689 longwave radiative fluxes ( $Q_S+Q_L$  (green)). Results are shown for 150 years of the NINT preindustrial control  
 690 (PiControl) simulation, evaluated over the Irminger Sea.

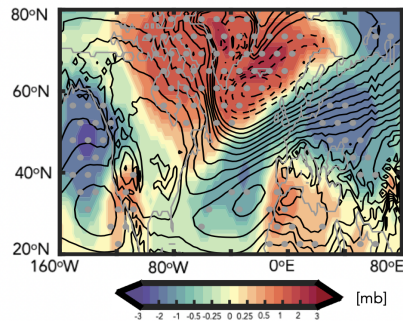


691 FIG. A2. Colors show the coupled atmosphere-ocean OMA - NINT (a,b) and LINOZ - NINT (c,d)  $4xCO_2$   
 692 changes in the DJF 300 hPa zonal winds. One ensemble member is used in the top panels, compared to four  
 693 members in the middle row. Panel e shows results from the atmosphere-only ensemble in which the time-evolving  
 694  $4xCO_2$  ensemble mean LINOZ ozone response is prescribed and the SSTs, SICs, and background  $CO_2$  are set to  
 695 preindustrial values. Left and right panels in the top and middle rows show the responses decomposed into “fast”  
 696 (i.e. years 5-20) (a,c) and “total” (i.e. years 100-150) (b,d) responses. Averages over years 40-60 are shown  
 697 for the prescribed SST and SIC experiments in panel e, which equilibrate much more rapidly, compared to the  
 698 coupled experiments. Black contours denote climatological mean preindustrial control DJF values (U contour  
 699 interval: 2 m/s) and stippled regions are statistically significant.

### DJF $\delta$ SLP $4\times\text{CO}_2$



LINOZ – NINT  
Coupled SST



LINOZ – NINT  
Fixed SST

700 FIG. A3. Top panel: Colors show the LINOZ minus NINT ensemble mean difference in the December-  
701 January-February (DJF) “fast” response of the sea level pressure to an abrupt quadrupling of  $\text{CO}_2$ . Results are  
702 shown for the fully coupled atmosphere-ocean simulations. Bottom panel: The ensemble mean response in sea  
703 level pressure in the experiments in which the time-evolving  $4\times\text{CO}_2$  ensemble mean LINOZ ozone response  
704 is prescribed and the SSTs, SICs, and background  $\text{CO}_2$  are set to preindustrial values. Black contours denote  
705 climatological mean preindustrial control DJF values (contour interval: 10 mb). Stippled regions are statistically  
706 significant.

707 **References**

- 708 Alexander, M. A., J. D. Scott, and C. Deser, 2000: Processes that influence sea surface temperature  
709 and ocean mixed layer depth variability in a coupled model. *Journal of Geophysical Research:  
710 Oceans*, **105 (C7)**, 16 823–16 842.
- 711 Ayarzagüena, B., and Coauthors, 2020: Uncertainty in the response of sudden stratospheric  
712 warmings and stratosphere-troposphere coupling to quadrupled CO<sub>2</sub> concentrations in CMIP6  
713 models. *Journal of Geophysical Research: Atmospheres*, **125 (6)**, e2019JD032 345.
- 714 Baldwin, M. P., and Coauthors, 2021: Sudden stratospheric warmings. *Reviews of Geophysics*,  
715 **59 (1)**, e2020RG000 708.
- 716 Bauer, S. E., and Coauthors, 2020: Historical (1850–2014) aerosol evolution and role on climate  
717 forcing using the GISS ModelE2. 1 contribution to CMIP6. *Journal of Advances in Modeling  
718 Earth Systems*, **12 (8)**, e2019MS001 978.
- 719 Bellomo, K., M. Angeloni, S. Corti, and J. von Hardenberg, 2021: Future climate change shaped  
720 by inter-model differences in Atlantic meridional overturning circulation response. *Nature Com-  
721 munications*, **12 (1)**, 1–10.
- 722 Booth, B. B., N. J. Dunstone, P. R. Halloran, T. Andrews, and N. Bellouin, 2012: Aerosols  
723 implicated as a prime driver of twentieth-century North Atlantic climate variability. *Nature*,  
724 **484 (7393)**, 228–232.
- 725 Butler, A. H., D. W. Thompson, and R. Heikes, 2010: The steady-state atmospheric circulation  
726 response to climate change–like thermal forcings in a simple general circulation model. *Journal  
727 of Climate*, **23 (13)**, 3474–3496.
- 728 Ceppi, P., and D. L. Hartmann, 2015: Connections between clouds, radiation, and midlatitude  
729 dynamics: A review. *Current Climate Change Reports*, **1 (2)**, 94–102.
- 730 Ceppi, P., G. Zappa, T. G. Shepherd, and J. M. Gregory, 2018: Fast and slow components of  
731 the extratropical atmospheric circulation response to CO<sub>2</sub> forcing. *Journal of Climate*, **31 (3)**,  
732 1091–1105.

- 733 Chiodo, G., and L. M. Polvani, 2019: The response of the ozone layer to quadrupled CO<sub>2</sub>  
734 concentrations: Implications for climate. *Journal of Climate*, **32** (22), 7629–7642.
- 735 Chiodo, G., L. M. Polvani, D. R. Marsh, A. Stenke, W. Ball, E. Rozanov, S. Muthers, and  
736 K. Tsigaridis, 2018: The response of the ozone layer to quadrupled CO<sub>2</sub> concentrations. *Journal*  
737 *of Climate*, **31** (10), 3893–3907.
- 738 Cowan, T., and W. Cai, 2013: The response of the large-scale ocean circulation to 20<sup>th</sup> century  
739 Asian and non-Asian aerosols. *Geophysical Research Letters*, **40** (11), 2761–2767.
- 740 DallaSanta, K., C. Orbe, D. Rind, L. Nazarenko, and J. Jonas, 2021a: Dynamical and trace gas  
741 responses of the quasi-biennial oscillation to increased CO<sub>2</sub>. *Journal of Geophysical Research:*  
742 *Atmospheres*, **126** (6), e2020JD034 151.
- 743 DallaSanta, K., C. Orbe, D. Rind, L. Nazarenko, and J. Jonas, 2021b: Response of the quasi-  
744 biennial oscillation to historical volcanic eruptions. *Geophysical Research Letters*, **48** (20),  
745 e2021GL095 412.
- 746 Delworth, T. L., and K. W. Dixon, 2000: Implications of the recent trend in the Arctic/North  
747 Atlantic oscillation for the North Atlantic thermohaline circulation. *Journal of Climate*, **13** (21),  
748 3721–3727.
- 749 Delworth, T. L., and F. Zeng, 2016: The impact of the North Atlantic oscillation on climate  
750 through its influence on the Atlantic meridional overturning circulation. *Journal of Climate*,  
751 **29** (3), 941–962.
- 752 Delworth, T. L., F. Zeng, L. Zhang, R. Zhang, G. A. Vecchi, and X. Yang, 2017: The central role  
753 of ocean dynamics in connecting the North Atlantic oscillation to the extratropical component  
754 of the Atlantic multidecadal oscillation. *Journal of Climate*, **30** (10), 3789–3805.
- 755 Eyring, V., S. Bony, G. A. Meehl, C. A. Senior, B. Stevens, R. J. Stouffer, and K. E. Taylor, 2016:  
756 Overview of the Coupled Model Intercomparison Project Phase 6 (CMIP6) experimental design  
757 and organization. *Geoscientific Model Development*, **9** (5), 1937–1958.
- 758 Garcia, R. R., and W. J. Randel, 2008: Acceleration of the Brewer–Dobson circulation due to  
759 increases in greenhouse gases. *Journal of the Atmospheric Sciences*, **65** (8), 2731–2739.

- 760 Gervais, M., J. Shaman, and Y. Kushnir, 2019: Impacts of the North Atlantic warming hole in  
761 future climate projections: Mean atmospheric circulation and the North Atlantic jet. *Journal of*  
762 *Climate*, **32** (10), 2673–2689.
- 763 Grise, K. M., and L. M. Polvani, 2014: The response of midlatitude jets to increased CO<sub>2</sub>:  
764 Distinguishing the roles of sea surface temperature and direct radiative forcing. *Geophysical*  
765 *Research Letters*, **41** (19), 6863–6871.
- 766 Isaksen, I. S., and Coauthors, 2009: Atmospheric composition change: Climate–chemistry inter-  
767 actions. *Atmospheric Environment*, **43** (33), 5138–5192.
- 768 Kantha, L. H., and C. A. Clayson, 2000: *Small scale processes in geophysical fluid flows*. Elsevier.
- 769 Kelley, M., and Coauthors, 2020: GISS-E2. 1: Configurations and climatology. *Journal of Ad-*  
770 *vances in Modeling Earth Systems*, **12** (8), e2019MS002 025.
- 771 Khatri, H., R. G. Williams, T. Woollings, and D. M. Smith, 2022: Fast and slow subpolar ocean  
772 responses to the North Atlantic oscillation: Thermal and dynamical changes. *Geophysical*  
773 *Research Letters*, **49** (24), e2022GL101 480.
- 774 Li, F., and P. A. Newman, 2022: Prescribing stratospheric chemistry overestimates southern hemi-  
775 sphere climate change during austral spring in response to quadrupled CO<sub>2</sub>. *Climate Dynamics*,  
776 1–18.
- 777 Lindzen, R. S., 1987: On the development of the theory of the QBO. *Bulletin of the American*  
778 *Meteorological Society*, 329–337.
- 779 Liu, W., A. V. Fedorov, S.-P. Xie, and S. Hu, 2020: Climate impacts of a weakened Atlantic  
780 meridional overturning circulation in a warming climate. *Science Advances*, **6** (26), eaaz4876.
- 781 Ma, L., T. Woollings, R. G. Williams, D. Smith, and N. Dunstone, 2020: How does the winter  
782 jet stream affect surface temperature, heat flux, and sea ice in the North Atlantic? *Journal of*  
783 *Climate*, **33** (9), 3711–3730.
- 784 Marshall, J., H. Johnson, and J. Goodman, 2001: A study of the interaction of the North Atlantic  
785 oscillation with ocean circulation. *Journal of Climate*, **14** (7), 1399–1421.

786 McLinden, C., S. Olsen, B. Hannegan, O. Wild, M. Prather, and J. Sundet, 2000: Stratospheric  
787 ozone in 3-D models: A simple chemistry and the cross-tropopause flux. *Journal of Geophysical*  
788 *Research: Atmospheres*, **105 (D11)**, 14 653–14 665.

789 Meinshausen, M., and Coauthors, 2020: The shared socio-economic pathway (SSP) greenhouse  
790 gas concentrations and their extensions to 2500. *Geoscientific Model Development*, **13 (8)**,  
791 3571–3605.

792 Meraner, K., S. Rast, and H. Schmidt, 2020: How useful is a linear ozone parameteriza-  
793 tion for global climate modeling? *Journal of Advances in Modeling Earth Systems*, **12 (4)**,  
794 e2019MS002 003.

795 Miller, R. L., and Coauthors, 2021: Cmp6 historical simulations (1850–2014) with GISS-E2. 1.  
796 *Journal of Advances in Modeling Earth Systems*, **13 (1)**, e2019MS002 034.

797 Mitevski, I., C. Orbe, R. Chemke, L. Nazarenko, and L. M. Polvani, 2021: Non-monotonic  
798 response of the climate system to abrupt CO<sub>2</sub> forcing. *Geophysical Research Letters*, **48 (6)**,  
799 e2020GL090 861.

800 Muthers, S., C. C. Raible, E. Rozanov, and T. F. Stocker, 2016: Response of the AMOC to reduced  
801 solar radiation—the modulating role of atmospheric chemistry. *Earth System Dynamics*, **7 (4)**,  
802 877–892.

803 Nowack, P. J., N. Luke Abraham, A. C. Maycock, P. Braesicke, J. M. Gregory, M. M. Joshi,  
804 A. Osprey, and J. A. Pyle, 2015: A large ozone-circulation feedback and its implications for  
805 global warming assessments. *Nature Climate Change*, **5 (1)**, 41–45.

806 O’Callaghan, M. J. D. S., Ameen, and D. Mitchell, 2014: The effects of different sudden stratospheric  
807 warming types on the ocean. *Geophysical Research Letters*, **41 (21)**, 7739–7745.

808 Orbe, C., and Coauthors, 2020: GISS Model E2.2: A climate model optimized for the middle  
809 atmosphere—2. Validation of large-scale transport and evaluation of climate response. *Journal*  
810 *of Geophysical Research: Atmospheres*, **125 (24)**, e2020JD033 151.

811 Orbe, C., and Coauthors, 2023: Atmospheric response to a collapse of the North Atlantic circulation  
812 under a mid-range future climate scenario: A regime shift in Northern Hemisphere dynamics.  
813 *Journal of Climate*.

- 814 Reichler, T., J. Kim, E. Manzini, and J. Kröger, 2012: A stratospheric connection to Atlantic  
815 climate variability. *Nature Geoscience*, **5** (11), 783–787.
- 816 Rind, D., J. Jonas, N. Balachandran, G. A. Schmidt, and J. Lean, 2014: The QBO in two GISS global  
817 climate models: 1. Generation of the QBO. *Journal of Geophysical Research: Atmospheres*,  
818 **119** (14), 8798–8824.
- 819 Rind, D., G. A. Schmidt, J. Jonas, R. Miller, L. Nazarenko, M. Kelley, and J. Romanski, 2018:  
820 Multicentury instability of the Atlantic meridional circulation in rapid warming simulations with  
821 GISS ModelE2. *Journal of Geophysical Research: Atmospheres*, **123** (12), 6331–6355.
- 822 Rind, D., R. Suozzo, N. Balachandran, A. Lacis, and G. Russell, 1988: The GISS global climate-  
823 middle atmosphere model. Part I: Model structure and climatology. *Journal of the Atmospheric*  
824 *Sciences*, **45** (3), 329–370.
- 825 Rind, D., and Coauthors, 2020: GISS Model E2.2: A climate model optimized for the mid-  
826 dle atmosphere—model structure, climatology, variability, and climate sensitivity. *Journal of*  
827 *Geophysical Research: Atmospheres*, **125** (10), e2019JD032 204.
- 828 Roach, L. A., E. Blanchard-Wrigglesworth, S. Ragen, W. Cheng, K. C. Armour, and C. M. Bitz,  
829 2022: The impact of winds on AMOC in a fully-coupled climate model. *Geophysical Research*  
830 *Letters*, e2022GL101203.
- 831 Romanou, A., and Coauthors, 2023: Stochastic bifurcation of the North Atlantic circulation under  
832 a mid-range future climate scenario with the NASA-GISS ModelE. *Journal of Climate*.
- 833 Shaw, T., and Coauthors, 2016: Storm track processes and the opposing influences of climate  
834 change. *Nature Geoscience*, **9** (9), 656–664.
- 835 Shaw, T. A., 2019: Mechanisms of future predicted changes in the zonal mean mid-latitude  
836 circulation. *Current Climate Change Reports*, **5** (4), 345–357.
- 837 Shepherd, T. G., 2014: Atmospheric circulation as a source of uncertainty in climate change  
838 projections. *Nature Geoscience*, **7** (10), 703–708.
- 839 Sigmond, M., and J. F. Scinocca, 2010: The influence of the basic state on the Northern Hemisphere  
840 circulation response to climate change. *Journal of Climate*, **23** (6), 1434–1446.



- 841 Simpson, I. R., T. A. Shaw, and R. Seager, 2014: A diagnosis of the seasonally and longitudinally  
842 varying midlatitude circulation response to global warming. *Journal of the Atmospheric Sciences*,  
843 **71 (7)**, 2489–2515.
- 844 Smith, D. M., and Coauthors, 2019: The polar amplification model intercomparison project  
845 (PAMIP) contribution to CMIP6: Investigating the causes and consequences of polar amplifica-  
846 tion. *Geoscientific Model Development*, **12 (3)**, 1139–1164.
- 847 Swingedouw, D., P. Ortega, J. Mignot, E. Guilyardi, V. Masson-Delmotte, P. G. Butler, M. Khodri,  
848 and R. Séférian, 2015: Bidecadal North Atlantic ocean circulation variability controlled by  
849 timing of volcanic eruptions. *Nature Communications*, **6 (1)**, 1–12.
- 850 Vallis, G. K., P. Zurita-Gotor, C. Cairns, and J. Kidston, 2015: Response of the large-scale structure  
851 of the atmosphere to global warming. *Quarterly Journal of the Royal Meteorological Society*,  
852 **141 (690)**, 1479–1501.
- 853 Visbeck, M., H. Cullen, G. Krahnemann, and N. Naik, 1998: An ocean model’s response to North  
854 Atlantic oscillation-like wind forcing. *Geophysical Research Letters*, **25 (24)**, 4521–4524.
- 855 Voigt, A., and T. A. Shaw, 2015: Circulation response to warming shaped by radiative changes of  
856 clouds and water vapour. *Nature Geoscience*, **8 (2)**, 102–106.
- 857 Yuval, J., and Y. Kaspi, 2020: Eddy activity response to global warming–like temperature changes.  
858 *Journal of Climate*, **33 (4)**, 1381–1404.
- 859 Zhai, H. L. J., Xiaoming, and D. P. Marshall, 2014: A simple model of the response of the Atlantic  
860 to the North Atlantic oscillation. *Journal of Climate*, **27 (11)**, 4052–4069.
- 861 Zhang, X., D. Waugh, and C. Orbe, 2023: Response of tropospheric transport to abrupt CO<sub>2</sub> in-  
862 crease: Dependence on the Atlantic Meridional Overturning Circulation. *Journal of Geophysical*  
863 *Research: Atmospheres*.